INFLUENCE OF MICROSTRUCTRAL CONSTITUENTS ON DEFORMATION AND FRACTURE OF Ni-BASE SUPER ALLOYS

A Thesis Report

Submitted in Partial Fulfilment of the Requirements for the Degree

of

Master of Engineering in Metallurgical Engineering

Department of Metallurgical and Material Engineering

Faculty of Engineering and Technology

Jadavpur University

Kolkata 700032

Session: 2017-2019

by

Avinash Kumar

Exam Roll no: M4MET19006

Registration no: 140897 of 2017-18

Under the guidance

Of

Dr. Amrita Kundu

Department of Metallurgical and Material Engineering

Jadavpur University

Kolkata 700032

and

Dr. H. N. Bar

Materials Engineering (MTE) Division

CSIR-National Metallurgical Laboratory, Jamshedpur-831007

MAY 2019

FACULTY COUNCIL OF ENGINEERING AND TECHNOLOGY

Department of Metallurgical and Material Engineering

Declaration of Originality and Compliance of Academic Ethics

I hereby declare that the work **"INFLUENCE OF MICROSTRUCTRAL CONSTITUENTS ON DEFORMATION AND FRACTURE OF Ni-BASE SUPER ALLOYS"** contains literature survey and original research work by the undersigned candidate, as a part of his Master of Engineering in Metallurgical Engineering studies. All information in this document have been obtained and presented in accordance with academic rules and ethical conduct. I also declare that, as required by these rules and conduct, I have fully cited and referenced all material and results that are not original to this work.

Place: Kolkata

Date:

AVINASH KUMAR

Examination Roll Number: M4MET19006

Registration Number: 140897 of 2017-18

Certificate of Approval

The foregoing thesis report is hereby approved as a creditable study of Engineering subject carried out and presented in a satisfactory manner to warrant its acceptance as a prerequisite for the Degree of 'Master of Engineering' in Metallurgical Engineering in the Department of Metallurgical and Material Engineering, Jadavpur university for which it has been submitted. It is understood that by this approval the undersigned do not necessarily endorse or approve any statement made, opinion expressed or conclusion drawn therein but approve the report only for the purpose for which it is submitted.

(SIGNATURE OF EXAMINERS)

COMMITTEE ON FINAL EXAMINATION FOR

EVALUATION OF THE THESIS

ACKNOWLEDGEMENT

This project I by far the most significant accomplishment in my life and it would have been difficult without people who supported me and believed me. I would like to thank Jadavpur University for giving permission to carry-out this research work at CSIR-National Metallurgical Laboratory (NML), Jamshedpur. I am grateful to Dr. S. Tarafdar for giving me sublime/upstanding opportunity to be part of acclaimed "CSIR-National Metallurgical Laboratory".

I would like to express my gratitude and appreciation to my institute guide assistant professor Dr. Amrita Kundu for her complete guidance, support and showing faith in me. Her patience and eye-opening suggestion are masterpiece of my tenure of this research work.

I am very much thankful to my CSIR-NML supervisor Dr. H. N. Bar for his encouragement and precious advises. I am obliged for showing faith and path towards in time completion of the research. I wish to express profound thanks to Dr, S. Sivaprasad Sr principal scientist at CSIR-NML for valuable suggestion and constructive comment. I am also thank to Dr. G. V. S. Murthy principal scientist at CSIR-NML, for valuable suggestion and providing me material for testing and furnace for heat treatment of sample. I would like to thank Mr, Parikshit munda, Scientist, CSIR-NML for helping me at various stage of project.

I would like to thank Rahul Chauhan, Lalit Kumar Gupta, Amit Kumar, Purshottam ,Sures Tudu, Rishikesh sastry and Vinod who helped me in various way, I would also like to acknowledge all my CSIR-NML friend especially, Suresh, Tuhin, Rashid, Shivam Bhupendra, who made me feel at home in Jamshedpur

I would also like to thank Mr. Manish Kumar Patel, Mr. Sayan Kalyan Chandra, Rahul Singh, and Jayanta Kumar Mahato, PhD scholars, at Jadavpur University for their unconditional and continuous support and assistance throughout my course of work

Lastly I would like to thank my parent for teaching me the value of hard work. Of course my parent's unconditional love and support is foundation of my will, and to my brother, who always take care of me irrespective of his problems and work pressure. Their Encouragement and never ending kindness made me everything easier to achieve.

	Title	Page
List of Figures		**v**
List of Tables		**vii**
Abstract		**01**
Chapter 1	**Introduction**	**02-05**
1.1	Introduction of research work	03
1.2	Purpose of the thesis work	03
1.3	Background	03
1.4	Fundamentals of Inconel 718	04
1.5	Properties of IN-718	04
1.6	Application of IN-718	05
1.7	Constituents of Nickel-Based Superalloys	05
Chapter 2	**Literature Review**	**06-17**
2.1	Heat Treatment Cycle	07
2.2	Solid Solution Strengthening	08
2.3	Microstructural Evolution	08
2.4	Aging Effects on Microstructure	09-11
2.4.1	The gamma phase (γ)	09
2.4.2	Gamma-prime phase (γ’)	09-10
2.4.3	Gamma double-prime phase (γ’’)	10-11
2.4.4	Delta phase (δ)	11
2.4.5	Carbide	11-12
2.5	Aging Effects on Hardness	12
2.6	Thermal Structural stability of Inconel 718 at higher temperature	12-13
2.7	Effect of aging on tensile strength and fracture	13-15
2.8	Fractography analysis of Inconel 718	15-17
Chapter 3	**Experimental Details**	**18-23**
3.1	Sample Preparation	19
3.2	Heat treatment cycle	19-20
3.3	Microstructural characterisation	20

3.4	Mechanical testing	21-23
3.4.1	Micro Hardness	21
3.4.2	Tensile test	21
3.4.3	Fractography	21
3.5	Fracture	21-23
3.5.1	Specimen Precracking	21-22
3.5.2	J-Integral test	23
Chapter 4	**Results and Discussion**	**24-39**
4	Microstructure	25-31
4.1	Optical Microstructure analysis	25-26
4.2	Scanning Electron Microscope analysis	27-31
4.3	Hardness test	31-32
4.4	Tensile result	32-36
4.4.1	Effect of heat treatment on the tensile strength	33
4.4.2	Effect of Aging on the yield and tensile strength	34
4.4.3	Effect of Precipitation number density on strength at room temperature and high temperature test	35
4.4.4	Effect of Aging on ductility at room temperature and high temperature test	36
4.5	Fractographic features	37-38
4.6	Fracture Experimental Results	38-39
Chapter 5	**Conclusions**	**40-41**
	Future Work Plan	**41**
References		**42-44**

List of Figures

Fig. No.	Description	Page No.
2.1	TTT diagram of different phases in Inconel 718	7
2.2	(a) Optical microstructure of as received 718 plus alloy (b) Microstructure of 718 plus alloy heat treated at 950ºC for 1 h	9
2.3	Crystal structure of γ phase	9
2.4	Crystal structure of γ' phase	10
2.5	Crystal structure of γ' phase	11
2.6	Fractography of IN-718	16
2.7	Freshly fractured carbide/matrix surface	16
2.8	HIP+1270°C/1 h/WQ and tested at room temperature; (b) HIP+955°C/1 h/WQ and aged and tested at room temperature	17
3.1	Schematic diagram of the tensile specimen.	19
3.2	Schematic diagram of the half (0.5) CT specimen.	19
3.3	Schematic diagram of the heat treatment cycles used in the present study	20
3.4	Set up for high temperature tensile test	21
3.5	Set-up used for pre-cracking of the specimens.	21
3.6	Half CT specimen during the room temperature J-test is in progress.	23
3.7	Waveform used to perform J-Test.	23
4.1	Effect of aging treatment on the grain size	25
4.2	Microstructures of the specimens	26
4.3	SEM image of the as-received Inconel 718	27
4.4	EDS mapping of the M0 specimen.	28
4.5	SEM image of M1 specimen	29
4.6	Twinning in the sample M0	29
4.7	Precipitates present in the sample M2	30
4.8	γ', γ'', δ and carbide precipitation of sample M3 and Table show EDS.	30
4.9	(a) δ precipitates with needle shaped (b) one variant appeared to have enveloped another variant (c) δ precipitates with plate morphology	31
4.10	Effect of heat treatment on the hardness	32
4.11	Tensile behaviour of various samples at room temperature	33

Fig. No.	Description	Page No.
4.13	Aging effect on the tensile strength at room temperature	34
4.14	Aging effect on the tensile strength at 650°C	34
4.15	Effect of precipitate number density on UTS at room temperature	35
4.16	Effect of precipitate number density on UTS at 650°C	35
4.17	Effect of Aging on the tensile elongation at room temperature.	36
4.18	Effect of Aging on the tensile elongation at 650°C temperature.	36
4.19	Fracture mode in tensile tests at (a) room temperature and (b) 650°C	37
4.20	Fig.4.20: (a) Crack initiation point during tensile test Fractographic image of sample M1 (b) at room temperature, (c) At 650°C	37
4.21	Fig. 4.21: J-R curve of M1, M2, M3, M4 and STD material obtained through experimental analysis	39
4.22	Fig.4.27: Effect of aging on the tensile elongation at room temperature	39

List of Table

Table No.	Description	Page No.
1.1	Composition of IN-718	5
1.2	Effects of elements in alloy 718	5
3.1	Test Matrix and Sample designation for tensile specimen and half CT specimen	21
4.1	Types of precipitate and composition obtained with heat treatment	31
4.2	Variation of tensile properties	32
4.3	Precipitate number density	35
4.4	Initiation fracture toughness (J_{Ic}) values of SHT & MHT IN-718 in room temperature	39

ABSTRACT

The objective of this thesis is to investigate how the mechanical properties mainly strength, ductility, micro hardness and fracture toughness of Inconel 718 are influenced by the microstructure evolution during heat treatment. Solution-annealed (SA) IN-718 were heat-treated at five different interval of time for obtaining different phases. The grain size and different precipitate number density analysis has been carried out by optical and scanning electron microscopy (SEM). The main intermetallic precipitates in IN-718 are (i) γ' having a composition Ni_3 (Al, Ti), a cubic crystal structure and cubic or spherical particle shape (ii) γ" having a composition Ni_3Nb, a BCT crystal structure and a lens-like disc shape (iii) δ having composition Ni_3Nb, an orthorhombic crystal structure and forming in needle shaped and plate shaped at grain boundary and extended in to grains.

Further the effect of heat treatments on the tensile and fracture properties of Nickel-based superalloy (IN-718) were studied at room temperature and at 650°C and a relationship of precipitate size, precipitate density and types of precipitate were established with strength and fracture toughness. Fractography of tensile sample has also been investigated in order to find out the fracture mechanism i.e. ductile or brittle and the way of propagation of crack either transgranular or intergranular are also investigated.

CHAPTER 1
INTRODUCTION

Chapter 1

Introduction

1.1 Introduction of research work

This thesis work is completion of the Master's programme, Metallurgy engineering at Jadavpur University in Kolkata. The thesis work has been performed at CSIR-National Metallurgy Laboratory, Jamshedpur. The objective was to investigate influence of microstructural constituents on deformation and fracture of Nickel base superalloy (IN-718). It was also focused that how different grain sizes and precipitate influences the mechanical properties, such as hardness, tensile strength and fracture toughness. Grain size measurement and precipitate density were done using LOM and SEM images. Heat treatment, polishing, Scanning Electron Microscope (SEM), Light Optical Microscope (LOM), tensile, fracture and fractography all test were conducted at the CSIR-NML.

1.2 Purpose of the thesis work

The thesis work was performed by investigating the influence of heat treatment on the mechanical properties of IN-718 on Macro and Micro level. At the macro level, tensile test, micro hardness tests and fracture test were performed. Hardness, Yield Strength, Ultimate Strength, modulus of elasticity, strain-hardening exponent and fracture toughness were found out. On the micro level the grain morphology like grain size after heat treatment using LOM was investigated. Variations in chemical compositions were investigated by SEM. An effort has been made to characterise the precipitate found out at different heat treatment process. Further a relationship was tried to establish between these precipitates and mechanical property.

1.3 Background

As one of the Nickel-base superalloys, Inconel 718 (IN718) was firstly designed and introduced to overcome the poor weldability of supealloys in 1960s. But now introduction of IN-718 is being used intensively in gas turbines and aero engines for discs and frames due to its excellent weldability. The focus of the thesis was on the Nickel based superalloy IN-718. Although different type of super alloys like Iron based, Cobalt based and different grade of Nickel based super alloy are available but IN-718 stands apart because capability to maintain good mechanical property and corrosion resistance up to 650°C. In addition, this alloy can be easily forged and welded. It contains a small amount of Carbon as well as very low levels of other constituents such as Si, Ta, Mn, Cu, S, B, P, and Mg. IN-718 has unique property that it can be processed as both wrought and cast product. Alloy 718 is the most widely used material for turbine disks and it is selected for many other applications as a high-strength material for temperatures up to 650°C.

The origin of the term Super alloy is rather obscure. Early works refer only to "Heat Resisting Alloys" or "High Temperature Alloys." These alloys are named as superalloys after a very popular television hero Superman [1]. During the 1939-1945 war a broad spectrum of high-temperature alloys from stainless steels to cermet were developed with the aim of improving the efficiency of gas turbines by increasing the melting temperature.

Super alloys are complex materials capable of maintaining their physical and mechanical properties at elevated temperatures compared to the properties measured at room temperature. Alloys developed for elevated temperature service in turbines and similar applications are based mainly on Iron, Cobalt and Nickel with such alloying elements as Cr, Nb, Mo, W, Ta, Al, Ti, and C and are known as superalloys. These alloys exhibit outstanding resistance to oxidation and hot corrosion as well as strength at elevated temperatures. Nickel is an ideal base for such alloys because of its high melting point, 1453°C, adequate corrosion resistance, and ability to dissolve to at least some limited extent. A number of other metallic elements which serve to strengthen it and also to improve its corrosion properties [2].

The major constituents of superalloys are mostly elements from the transition metal group. Iron and Cobalt are metals with FCC structure at certain temperature and Nickel have FCC structure for all temperature. Depending upon the base metal these can be classified as Nickel base, Cobalt base and Nickel-Iron base Superalloys [3]. Nickel base alloys are the most complex, most widely used for the hottest parts and most preferred superalloys. Nickel based superalloys used in vast applications mainly subjected to high temperature due to the principle characteristic of Ni as an alloy base having high phase stability of FCC Nickel matrix along with strength retention up to $0.7T_m$. Diffusion rate of Ni is very low which leads to microstructural stability in the alloy at elevate temperatures. Cobalt alloys have higher melting points than Nickel (or iron) alloys [4]. This gives them the ability to absorb stress to a higher absolute temperature. Cobalt alloys give superior hot corrosion resistance to gas turbine atmospheres due to their high chromium content. Cobalt alloys show superior thermal fatigue resistance and weldability over Nickel alloys. Superalloys containing substantial quantities of both Ni & Fe form a distinct class of superalloys known as Nickel-Iron base Superalloy. The austenitic FCC matrix of superalloys has extended solubility for some alloying elements, excellent ductility and favourable characteristics for precipitation of effective strengthening phases. Superalloy density is influenced by alloying additions- Aluminium, Titanium, and Chromium reduces density, whereas Tungsten, Rhenium, and Tantalum Increase it. The corrosion resistance of superalloys depends primarily on the alloying elements added, particularly Chromium, and Aluminium and the environment experienced [5].

1.4 Fundamentals of Inconel 718

Inconel 718, a Nickel-Iron-base superalloy was developed by International Nickel Corporation in the 1950s and found many applications in turbine components [6]. Although Inconel 718 has been introduced for a long time ago, it is still widely used in many applications, especially under high-temperature environment such as the turbine engine, military aircraft, power generation, and marine propulsion and heat treatment equipment's [1].

1.5 Properties of IN-718 [1-5]

- High yield and ultimate strength
- Good creep and rupture strength
- High resistance to fatigue
- Possess long time strength and toughness at higher temperature
- Confinement of corrosion and oxidation resistance up to elevated temperature
- Lower thermal conductivity or higher electrical resistivity

1.6 Application of IN-718 [1-5]

- Gas turbine hot section components
- Space shuttle main engine
- Metal processing and heat treating equipment (trays, furnace, mufflers, conveyor belt, fixture)
- Heat exchanger
- Cryogenic storage tanks
- Nuclear power plants
- Chemical and Petro-chemical industries

1.7 Constituents of Nickel-Based Superalloys

The microstructure of Nickel-based superalloys consists essentially of a γ matrix phase, in which a fine, uniform dispersion of γ', one or more carbide phases and usually at least one other minor phase are precipitated. One of the most important factors dictating the microstructure is the overall composition of the material because in most alloys the alloying elements are completely soluble in the Nickel up to a limited temperature range below the solidus temperature. The solid solution of alloying elements in Nickel, the γ-phase, is extremely important in governing the microstructure. Therefore, some attention must be paid to the γ-phase. As constant reference will be made to commercial alloys throughout the review, the compositions of a number of such alloys are given in Table 1.1 [2].Effect of alloying element on IN-718 is discussed in Table 2 [7].

Table 1.1 Element (Weight %)

Ni	Cr	Fe	Mo	Ti	Nb	Co	Mn	Cu	Al	C	Si
50.0-55.0	17.0-21.0	18.0-20.0	2.8-3.3	0.65-1.25	4.75-5.5	≤1	≤0.35	≤0.3	0.2-0.8	≤0.08	≤0.35

Table 1.2 Effects of elements in alloy 718

Elements	Effects
Co	Solid solution strengthening by raising solvus temperature of γ'
Mo	Solid solution strengthening
Cr	Oxidation resistance and hot corrosion resistance at high temperatures
Fe	Solid solution strengthener
Ti	Carbide and hardening precipitates and/or intermetallic former
Al	Oxidation resistance at high temperatures
B	Enhances creep-rupture properties by GB morphology change/causes GB segregation

CHAPTER 2
LITERATURE REVIEW

Chapter 2

Literature review

2.1 Heat Treatment Cycle

In order to get good ductility, good formability, yield, tensile and creep rupture, as-received material was given the standard heat treatment, viz solution treatment at mainly two temperatures 980°C and 1040°C [8, 9] for different time and water quenched (WQ) or Furnace cool. It is apparent from the TTT diagram that the approximate temperature range for various phases will be like [5, 6, 10, 11].

γ' = 593.33°C to 704.44°C

γ'' = 704.44°C to 898.89°C

δ = 871.11°C to 1010°C

The solvus temperature for γ'/ γ'' is expected from TTT diagram (Figure 2.1) to be 886°C while δ solvus temperature is considered to be 1027°C [6, 12]. Above the solvus temperature the phases get dissolve completely in the matrix. Below solvus line the phase get unstable due to increase in driving force and so the rate of nucleation of the corresponding phase will increase. Moreover as the rate of diffusion is exponential function of temperature, rate of diffusion will decrease. Thus transformation of the precipitates depends on the overall effect of rate of diffusion and rate of nucleation. The solution treatment will allow the intermetallic and grain boundary precipitates to dissolve in the matrix and also permits required diffusion. Rapid quenching helps to get supersaturated solid solution and will prevent formation of equilibrium precipitates due to natural ageing. γ' and γ'' precipitates are formed simultaneously in the 550-600°C temperature range for long-time aging at the opposite, they are formed always simultaneously in the temperature range of 700°C to 900°C for short-time aging [13].

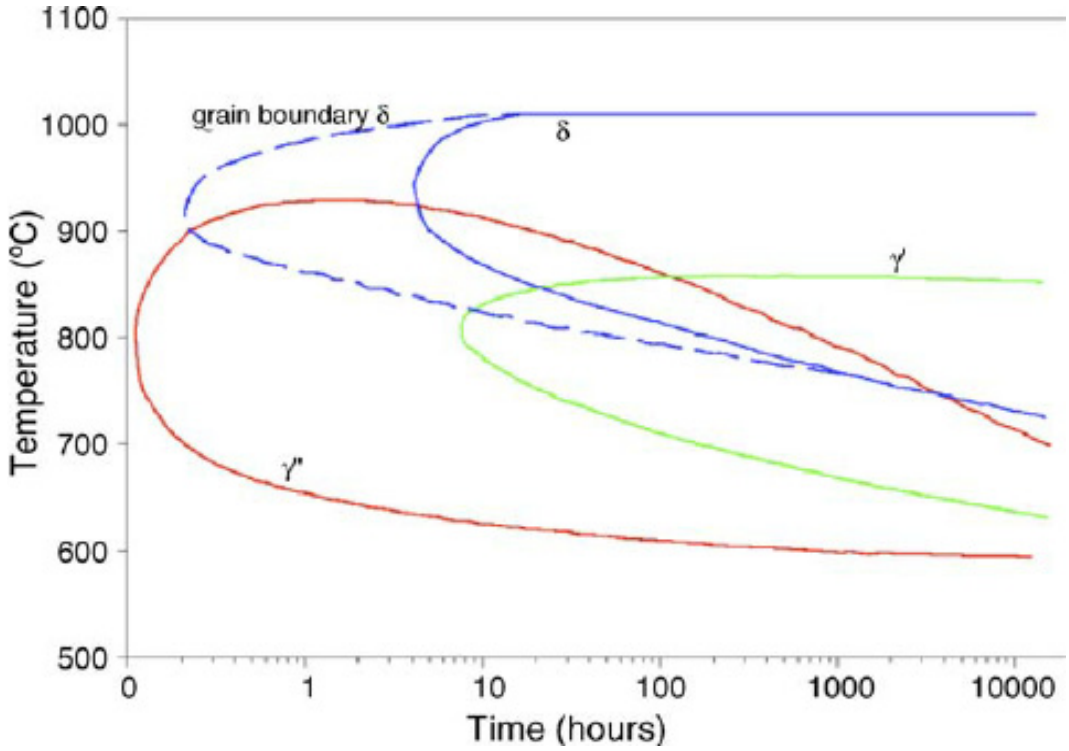

Fig.2.1: TTT diagram of different phases in Inconel 718 [14]

2.2 Solid Solution Strengthening

Majority of Superalloys are strengthened by solid solution strengthening or precipitation Strengthening and the upper temperature limit for alloy used is governed by the base metal as well as the type and volume of the intermetallic precipitates formed by the combination of the base metal and the alloying element. In IN-718, γ'' is the commonly observed strengthening phase, which results in high temperature strength of the alloy up to 650°C. At higher ageing temperature "the metastable γ" phase will dissolve and will transform to stable δ-phase. The growth and dissolution of the precipitate particles are significant as they control the long-time mechanical properties of the alloy. By modifying the composition, with a variation in Al, Ti and Nb content as mentioned earlier one can get compact morphology having higher thermal structural stability. . Kinetics [15] of coarsening of γ" follows the time-law prediction of diffusion-controlled growth theory, based on the growth theory of Lifshitz, Slyozov [16] and Wagner[17]. The compact morphology [18] (γ'+ γ") in which cube shaped γ' precipitates are coated with γ" precipitates on their six faces. It is expected that dissolving can be identified from BCT structure of only three sides. Also in some region the part opposite to dissolved γ'' precipitates; appears to be dissolving in a form observed superfluous smaller part. However on ageing for longer duration of time, the compact morphology differs with γ' of a semi-spherical shape rather than of a cubic shape and only one of the γ'' is observed on the interface. This is due to destruction of compact morphology with increase in ageing time and once compact morphology is destroyed, rapid coarsening occurs due to relaxation of constraining force of γ" and γ". As mentioned earlier, during dissolution, there remains only one side of γ" which combines with γ'. These larger γ" precipitates are attributed to rapid coarsening at longer duration of thermal exposure. Finally γ" is completely separated with γ' and grows rapidly in form of platelet like structure. Thus one can conclude that at lower temperature and shorter time of exposure (i.e. during initial stage of ageing), γ' and γ" is in compact morphology, constrain to each other and grows schematically forming a sandwich like structure. After dissolution of strengthening phase and with the formation of stable orthorhombic delta phase, strength of alloy decreases as delta phase is incoherent with matrix and hence releases the effective shear strain which restrict the dislocation movement.

2.3 Microstructural Evolution

A number of studies have been carried out to observe the microstructural evolution during high temperature exposure of alloy 617. The microstructure of 718 plus in as received hot-rolled condition consists of FCC austenitic-matrix with an average grain size of 50 μm. Fig. 2(a) shows the optical micrograph of the as received IN-718 alloy. It can be seen that precipitates with round-to-blocky morphology are randomly dispersed within the microstructure [19]. After SA at 950^{o}C for 1 hour microstructure of 718 plus alloy, it can be seen that needle like δ phase is observed on the grain boundaries and occasionally intra-granularly on the twin boundaries and also seen in the microstructure; round and blocky shaped MC type carbide particles are randomly distributed. Ti-rich carbo-nitride particles can be also observed shown in Fig. 2(b). Various precipitates with different sizes have been found in this alloy. Large primary carbides including Mo-rich M_6C and Ti-rich M(C, N) and small Cr-rich $M_{23}C_6$ secondary precipitates were distributed within the austenitic grain and grain boundaries have been shown in Fig. 2(b) [20].

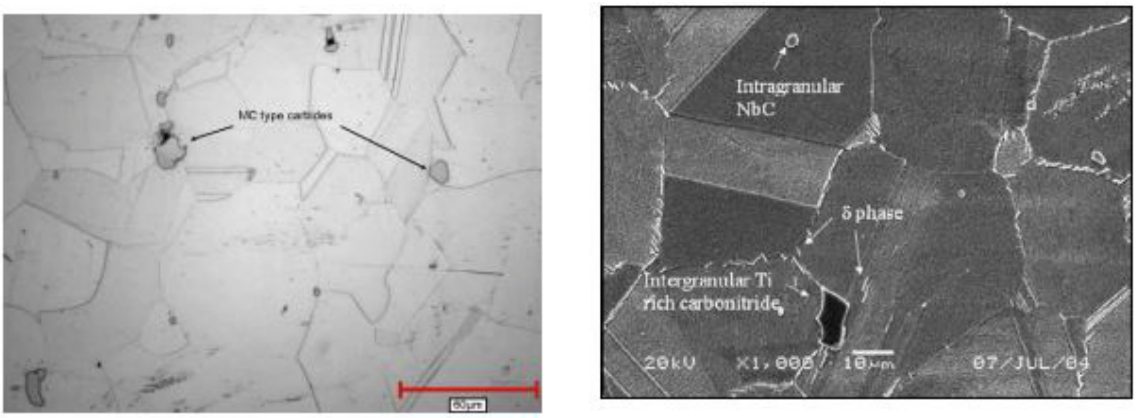

Fig.2.2: (a) Optical microstructure of as received 718 plus alloy[19], (b) Microstructure of 718 plus alloy heat treated at 950ºC for 1 h [20].

2.4 Aging Effects on Microstructure

The precipitation in In-718 extensively studied because of their ability to retain properties at high temperature. Amount and types of precipitates depends upon aging time and temperature.

2.4.1 The gamma phase (γ)

The gamma phase is nonmagnetic with a face centred cubic (FCC) structure. Illustration is shown in Fig.2.3 [21]. Nickel allows alloying with solid solution strengthening elements without losses in phase stability. The alloy elements composing the gamma matrix mainly belong to Group V, VI and VII. Alloying elements expand the lattice parameter of Ni, the rate of expansion per solute addition being the greatest for Nb, W, and Mo, and the least for Co, Cr, and Fe. Hence, one would expect the refractory metals, Nb, W, and Mo to be potent solid-solution strengtheners as these would interfere most with lattice periodicity. Indeed alloy development programs have proven Mo and W to be extremely potent solid-solution strengtheners in Ni-based alloys [22].

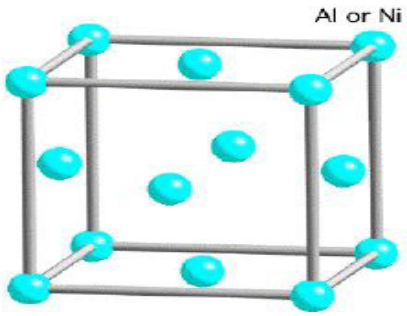

Fig.2.3: Crystal structure of γ phase [21]

2.4.2 Gamma-prime phase (γ')

The gamma prime phase formed from Group III, IV and V elements. The structure of gamma prime is FCC having a composition of $Ni_3(Al,Ti)$ and a cubic ($L1_2$) crystal structure [23] (figure 2.4). The amount of γ' present is critical to the performance of the superalloy, but it is dependent on temperature. The structure of superalloys is chemically dynamic, even at room temperature, and can only be observed temporarily [24]. Not only does the amount of γ

depend on the temperature at which the material is cast or wrought, but the material is also reacting when the superalloys are exposed to the high temperatures of operation. The precipitation of γ' in the matrix is a continuous process: the phases are constantly reacting and interacting. There are three main stages to precipitation, the nucleation of the precipitate γ' in the γ matrix, followed by growth and then ripening, or ageing [25]. From a study of the equilibrium relationships in the systems Ni-Cr-Ti, Ni-Cr-Al, and Ni-Ti-Al, Ni_3Al dissolves considerable amounts of Cr and Ti, and some Ni. Up to 60% of the Al atoms could be replaced by Ti in Ni_3A1 with only a slight increase (less than1%) in the lattice parameter. In general, the effect of the replacement of part of the Al with Ti in Ni-Cr and Ni-Cr-Co-based alloys is to decrease the rate of growth of the γ'-precipitates and, thus delay over aging. Also, Ti is more significant than A1 in imparting strength at higher temperatures [22] probably due either to the decreased rate of growth of the precipitates or to a higher solution temperature of Ni_3(A1, Ti) versus that of Ni_3AI. Because the Titanium bearing alloys are less prone to over aging and are more stable at higher temperatures. The volume fraction of γ' in commercial alloys varies approximately between 20 and 60% depending upon the alloy system [20], the amount of γ' increases with increasing total (A1+Ti) content of the alloy and with decreasing

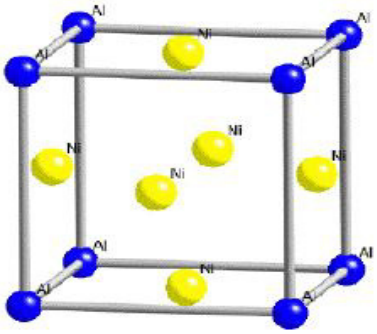

Fig.2.4: Crystal structure of γ' phase [21]

aging temperature. Initially observed as spherical precipitate then as cubes depends upon lattice mismatch, if lattice mismatch is up to 0.2% favours spherical formation where as 1% mismatch promotes cubical and if greater than 1.25 % leads to platelets or elongated.

2.4.3 Gamma double-prime phase (γ'')

The precipitate phase gamma double prime (γ") is the principle strengthening phase in IN-718 having a composition Ni_3Nb and a Body Centred Tetragonal (BCT) ($D0_{22}$) crystal structure [23] (Figure 2.5). The γ" precipitates as disk shape nature [26] usually have a length 5 to 6 times its thickness and size is less than 200A°. The γ" and γ' phase grow with higher temperature and long-time exposure at low temperature, a transition of γ' and γ" to delta phase occurs slowly at lower temperature, but the reaction occurs faster or sooner at the higher temperature. Hence it has been found that γ' and γ" phase grow in a sandwich-like morphology indicating a precipitation of the phases. However γ" can be separated from γ' using dark field TEM as dark field image of γ'' is brighter than that of γ' [5].

The Ni-base superalloys currently used at the highest service temperatures are strengthened by cubic Ni_3Al gamma prime (γ′) precipitates. In contrast, the most widely used superalloy, Inconel 718, is reinforced by tetragonal Ni_3Nb gamma double prime″)(γ precipitates. The additional strengthening conveyed ƀyoγer γ′ is a function of the coherency of the precipitates with the matrix and the distortion caused by the c-axis of the tetragonal γ. However, such alloys are limited to lower-temperature applications, as above

650°C the γ″ phase decomposes to the thermodynamically stable δ phase, with a concomitant deterioration in strength.

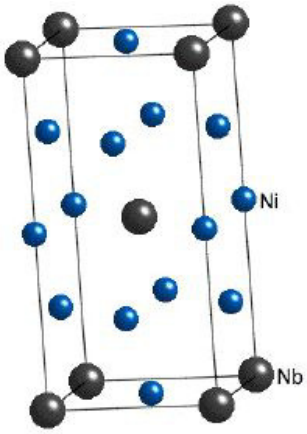

Fig.2.5: Crystal structure of γ' phase [21]

2.4.4 Delta phase (δ)

In Inconel 718, phase formation occurs over the 650–980°C temperature range with a platelet and niddle shape morphology [27]. Due to over ageing in Ni-Fe base superalloys, the metastable phase γ" coarsens and transforms to stable delta (δ) [28], having composition Ni_3Nb and an orthorhombic (D0a) crystal structure [23]. On holding γ" at high temperature for longer time eventually will lead to growth of δ -phase at the expanse of γ". Kirman and Warrington [29] showed that the growth of *δ* at the expense of γ'' precipitates mainly at grain boundaries and a high volume fraction of small γ" precipitates within the grains. They also shown that both the γ' and γ" phases occur when 1.8Ti and 3.5Nb were added, but when the Ti content was increased to 3.5Ti only the γ' phase was obtained, while increasing the Nb content to 6Nb allowed only the γ'' phase to form. At relatively lower temperatures, δ phase nucleates at austenite grain boundaries as well as coherent and incoherent twin boundaries, while at higher temperatures they precipitate intragranularly [30]. The delta phase is found mostly as plates growing on the (111) planes or nucleating on the grain boundaries and is associated with loss of strength in this alloy. Also δ-phase in the grain boundaries is used to control grain size in wrought material, improve grain boundary sliding, creep rapture strength and seems to be also important for notch ductility [5, 31].

2.4.5 Carbide

Carbide formation Ni-based superalloys are required to stabilize the structure against high-temperature deformation**.** This is accomplished by the formation of carbide networks at the grain boundaries. These networks inhibit grain-boundary motion, thus increasing creep and stress-rupture properties. The effects of carbides upon high-temperature properties are dependent upon the type of carbide present and its morphology [32]. The most stable carbide found in Ni-based superalloys is the MC carbide, where M usually represents Ti, although part of the Ti may be substituted for by Nb, Ta, W, Mo, and Cr, depending upon alloy composition. The MC carbide has an FCC crystal lattice. Most commercial precipitation-hardenable Ni-based alloys contain MC in their microstructure. The lump MC carbides, which appear within the grain boundaries, are helpful for the improvement of stress rupture life, and they can effectively prevent the grain-boundaries sliding [33, 34]. MC is usually stable to temperatures close to the fusion temperature. MC Carbide replace by M_6C and

$M_{23}C_6$ during high temperature service. $M_{23}C_6$ carbide form in the range of 760-980°C, these carbide have a complex cubical structure and generally form on grain boundaries and M6c carbide form in the range of 815-980°C.

2.5 Aging Effects on Hardness

Slama [35] suggested that hardness change as a function of the tempering duration at different temperatures. At 680°C, the temperature is sufficiently high to allow the diffusion to be operative and to induce a rapid strengthening; consequently, the volume fraction of precipitates will be more important and the maximum value will be the highest (HV=500). At 750°C, the diffusion rate is still higher and the hardening kinetics is faster, in such a way that after a 4-h tempering, the hardness is equal to 465. The coarsening of precipitates leads rapidly to a hardness decrease. In fact, the higher the duration of the isothermal soaking the lower is the hardness value. Cozer and Pineau [36] found that IN-718 have high hardness value which has high amount Al + Ti + Nb.

2.6 Thermal Structural stability of Inconel 718 at higher temperature

Thermal stability of IN-718 was evaluated by the change in microstructure and mechanical properties after long time thermal exposure. The major microstructural changes due to thermal exposure included formation of γ' and γ" strengthening phases, dissolution of metastable γ" phase and finally formation and growth of stable orthorhombic δ-phase from the metastable γ" phase [37]. A Time-Temperature-Transformation (TTT) diagram for IN-718 is shown in Fig.4 [38]. From the TTT diagram one can conclude that γ" has a wide range of formation temperature and formation of γ" takes place during ageing. The favourable condition for the nucleation and growth of γ" on γ', is the flat faces of FCC γ' precipitates and initial size of the γ' precipitates before the formation of γ". Thus compact morphology (γ'+γ'') can only be obtained if γ' precipitates has reached to minimum critical size. Explanation for the occurrence of compact morphology from γ' precipitate is given as under and the figure for the same is shown in Fig.5 [36]. At first it was expected that at given temperature small size of γ' particle has already precipitated when a γ'' particle is nucleated on it. The probability of nucleation of γ'' particle on FCC crystal having six faces may not be the same and hence it is assumed that γ'' is preferentially formed on one of the face. The γ" precipitate particle will overlap the γ' precipitate if there is small increase in dimension. As γ" (Ni_3Nb) precipitate is rich in Nb content, the concentration of Nb around γ' precipitate will be lowered. This zone is called diffusion zone. Finally after formation of small particle at higher ageing temperature the dimension of γ' precipitates increase over the critical size resulting in increase rate of precipitation easily along all the six face of γ' precipitates. Thus two main condition necessary for the formation of compact morphology are relative position for the start of and γ'' precipitation in TTT diagram and the kinetic of γ' growth. After formation of γ'' precipitates the growth rate of γ' is slowed down. For the appearance of γ'' precipitates there is the existence of the critical temperature corresponding to the critical size of γ' precipitates as shown in Fig.6. Again the incipient γ'' precipitation curve is dependent on the sum of the amount of Ti, Al, Nb, and also on the ratio (Ti+Al)/Nb. If this ratio is increased then the rate of γ' precipitation will be increased in comparison to γ'' precipitates. Moreover for the formation of stable compact morphology a critical (Ti+Al)/Nb ratio between 0.9 and 1 has been observed. But John P. Collier [39] suggest that this ratio approximately equal to 0.7. Preliminary experimental results suggest that allowing the atomic

percent of Aluminium and Titanium to equal that of Niobium may result in a more thermally stable γ''. Also at lower temperature γ'' is found to be always associated with γ' precipitates in sandwich like structure. Pre-treatment and heat treatment have no influence on the relative fraction of γ' and γ'' phases Inconel 718; the ratio of γ' to γ'' is approximately the same under different pre-treatment conditions and can be taken as a constant equal to 3 [40].

2.7 Effect of aging on tensile strength and fracture

K M Chang and A H Nahm [41] finds that One subgroup of precipitation strengthened Nickel based superalloys are those that are primarily strengthened by the γ' phase [2], e.g. 718 Plus [41]. Another group of precipitation strengthened Nickel-based superalloys are those which are principally strengthened by the γ" phase (eg. IN-718). Within the literature, it seems that the temperature range in which the δ phase nucleates within is disputed, with some authors mentioning it to be between 700 and 1000°C [23] or 750‑1020°C[42]. The solvus temperature of the δ phase is also uncertain as it has been reported to be in the range of 990‑1020°C [43]. The differences in δ phase solvus temperature is said to be due to the fluctuations in chemical composition of the alloy, with the Niobium content having the most influence on the δ phase solvus temperature [43]. The fastest rate of δ phase precipitation occurs at approximately 900°C [23, 42]. It usually nucleates and precipitates starting at the grain boundaries of the γ phase [23] through a discontinuous reaction [44]. It then grows into thin plates along the grain boundary and eventually elongating into the phase grains. δ phase precipitation can also occur intragranularly when γ" phase is present [23].

WD Cao and R Kennedy[45] shown that the phase stability of the γ' phase is heavily linked to the ratio of aluminium to titanium (Al/Ti). At low values of Al/Ti, small quantities of γ' are present whereas large amounts of δ and η phases are present within the microstructure, which shows that the thermal stability is low. The contrary is also true; at high Al/Ti values, large quantities of γ and low amounts of δ and η phases are present in the microstructure, therefore meaning a high γ' high thermal stability [39, 46]. Furthermore author arose as an effect of increasing the Al/Ti and (Al+Ti)/Nb ratios in Inconel 718. Prior to its dissolution, coarsening of γ" takes place. By slowing down the γ" coarsening rate, the thermal stability of γ" is improved. The adjusted Al/Ti and (Al+Ti)/Nb ratios in Ti alloy enabled a lower coarsening rate of the metastable γ" as well as a delay in the precipitation of the stable δ phase [47]. Guo et al [48] and Xu et al [49] found that the coarsening rates of γ' and γ" are much slower in modified 718-type alloys with higher values of (Al+Ti)/Nb and Al/Ti ratios. In addition, less δ phase was found within these alloys. Therefore, Guo et al and Xuet al. both attribute the increased thermal stability from higher elemental ratios to the slower γ' and γ" coarsening rates, rather than an increase in γ' precipitation at the expense of γ" which was proposed by Collieret al. [46] and Tien et al. [50]. However, Guo et al [48] mentions that the γ" coarsening rates are slower than γ' whereas Xu et al.[49] contradicts this by stating that the γ' coarsening rate is slower than γ". Cozar and Pineau [36] and Andrieu et al. [51] found that by increasing these values and aging at 750°C for long periods of time, a compact morphology of the γ' and γ" phases is obtained. The compact morphology consists of cube shaped γ' particles covered on all sides by γ". This occurs due to γ'' nucleating and coarsening on γ' particles. This morphology is very stable at prolonged aging times which is the reason for the enhanced thermal stability of the superalloy.

Shih-Hsien Chang and Shih-Chin Lee showed that a solution temperature of 1020°C is optimum. The Laves and δ phase can complete solution after 1020°C, 1 h solid-solution treatment. They discussed the effect of various aging treatments for as-HIP treated 718 alloys. In the experiment, seven different aging treatments were used: 720°C for 2, 4, 8 and 16 h, furnace cooled to 620°C, soak for 8 h, and air cooled to room temperature; 720°C for 8 h, furnace cooled to 620°C, soak for 2, 4, 8 and 16 h, and air cooled to room temperature. Experimental results showed that 1020°C solid-solution, 720°C for 8 h and 620°C for 4 h of aging treatment for as-HIP treated 718 alloys is optimum. All the precipitations are MC carbides; the dimension of γ" precipitations is 30.41 nm, which with a maximum tensile strength (1407.2 MPa) and elongation (14.5%) at room temperature[52]. Qingbo Jia and Dongdong Gu reported on the densification, microstructure and properties of selective laser melting (SLM) processed Inconel 718 parts. They conclude that microstructures of SLM-processed Inconel 718 parts experienced successive changes: coarsened columnar dendrites – clustered dendrites – slender and uniformly distributed columnar dendrites, on increasing laser energy density and the optimally prepared Inconel 718 parts had a uniform microhardness distribution with an increased mean value of 395.8$HV_{0.2}$.Bilal Hassan and Jonathan Corney are explored impact of grain boundary precipitation on the mechanical properties. They control Grain boundary precipitates and the grain size in Inconel 718 during hot working processes. There review considers the background of grain boundary precipitation including the effect of the thermal stability of γ' and γ" phases. In addition, the effect of stress on the grain boundary phases and their precipitation kinetics in different conditions are also included [53].

Byun and Farrell [54] investigated tensile properties of Inconel 718 alloy in solution-annealed (SA) and precipitation-hardened (PH) conditions have been temperature neutron irradiation up to 1.2 dpa. They found that In the SA IN718, an almost threefold increase in yield strength at 1.2 dpa and the material retained a strong strain-hardening capability and a high uniform ductility of more than 20%. However, the originally much stronger PH IN718 displayed little radiation-induced hardening in yield strength and significant softening in ultimate tensile strength. Trosch and Strobner, [55] compared selective laser melting (SLM) to forging and casting regarding differences in microstructure and mechanical properties of Inconel 718. Tensile mechanical properties of SLM Inconel 718 samples are superior to conventionally produced specimens at room temperature and 450°C. By continuous optimization of the microstructure with respect to δ-phase distribution and anisotropy, the mechanical properties (e.g. UTS, Rp0.2, ϵf) can be further improved at temperatures above 450°C

Xiaoming Zhao and Jing Chen [56]through heat treatment, the tensile strength of LRF GA IN718 samples is comparable with wrought IN718, which is approximately 1.5 times of that of the as-deposited samples. But there is a remarkable decrease in ductility. Both the rupture life and ductility of LRF GA IN718 have been found to be much less than the specified figures for cast IN718. The average hardness (HRC41) for heat-treated samples increased remarkably on comparison with as-deposited samples (HRC17). Azer and Ritter [57] studied and compared tensile properties of the laser-deposited IN718 alloy under the conditions of as deposit, direct age, solution treatment and age (STA), and homogenization followed by STA. They found that the as-deposited alloy without any heat treatment remains soft and exhibits low tensile strength and good ductility (16.2 pc). The tensile strength was increased dramatically (100 pct improvement yield stress) and shown to be equivalent to wrought

material after direct age due to the precipitation of the γ' and γ" strengthening phases in the matrix; however, the ductility of the direct-aged material is reduced substantially to 8.4 pct due to fine Laves particles that remain at the interdendritic regions. These regions subsequently became relatively weaker sites, initiating fractures during tensile testing. Standard STA heat treatment has transformed most of the Laves phases to fine acicular d phase at the interdendritic regions. Good ductility (16.0 pct) and slightly lower tensile strength (about 8 pct lower) were obtained from the STA treatment compared to the direct-aged condition. The low Nb bands formed at the deposit layer interfaces and the resultant grain size growth in these regions during the solution heat treatment seem to account for the slightly reduced tensile strength compared to the direct-aged material. The homogenized STA heat treatment completely dissolved the Laves phase but enabled substantial grain growth with isotropic appearance. As a result, this heat treatment produced the best ductility (19.9 pct), the tensile strength decreased 10 pct as compared to the direct-aged material. Aguimaraes and Jonas [58] suggested that below 975°C for Inconel 718, dynamic recovery is the softening mechanism occurring during deformation from 975 to 1090 ~ at strain rates between 9.3 x l0 $^{-4}$ s^{-1}and 9.3 x 10 $^{-2}$ s^{-}for Inconel 718, dynamic recrystallization is observed after 0.4 strain. Tabernero and Lamikiz [59] compared wrought IN-718 and IN-718 component built by laser cladding They found further precipitation hardening of cladded IN-718 component higher tensile strength and ductility increments as much as 100%.because of homogenisation of the microstructure of the deposited material. Dong and Xie proposed that e stress-rupture life increased with decreasing sulphur and increases with increasing with P, Mo, and Nb. Further Cao and Kennedy [60] and Xie et al. [61] have reported that Phosphorus seems to be beneficial for the stress-rupture life and ductility improvement in alloy 718.

2.8 Fractography analysis of Inconel 718

Fractography obtained from the tested specimens shows the micropores and microcracks at the position close to sample surface, indicating a fact that primary cracks originate from micropores and propagate to surrounding material, as shown in Figure 2.6(a). Fracture surface of dendrite without micropore defect remains the morphology of primary and secondary dendritic arm, as shown in Figure 2.6(b). Secondary crack in original cracking site connects micropores one by one, revealing that the level of stress easily exceeds the strength bearing limitation of the material in this region, as shown in Fig2.6(c). The Smooth surface of microporosity is comparable to dendrite fracture surface which consists of a large number of dimples and cleavage planes. High magnification of SEM picture (see Fig 2.6(d) provides the evidence to a fact that narrows interdendritic regions on the surface of microporosity. give birth to initial cracks [62]. Litao and Wenru Sun[61] found two types of phases near the crack, the first is rich in Nb and identified as MC-type carbide by considering their morphology and the second are rich in Nb, Mo, Cr, and identified as Laves phase [63]. J.X. Dong and X.S. Xie found that carbides are apparently a major source for crack nucleation. The carbide/matrix interface may possibly be weakened by impurity segregation and, thus, assist the fracture initiation process as shown in figure 2.7.

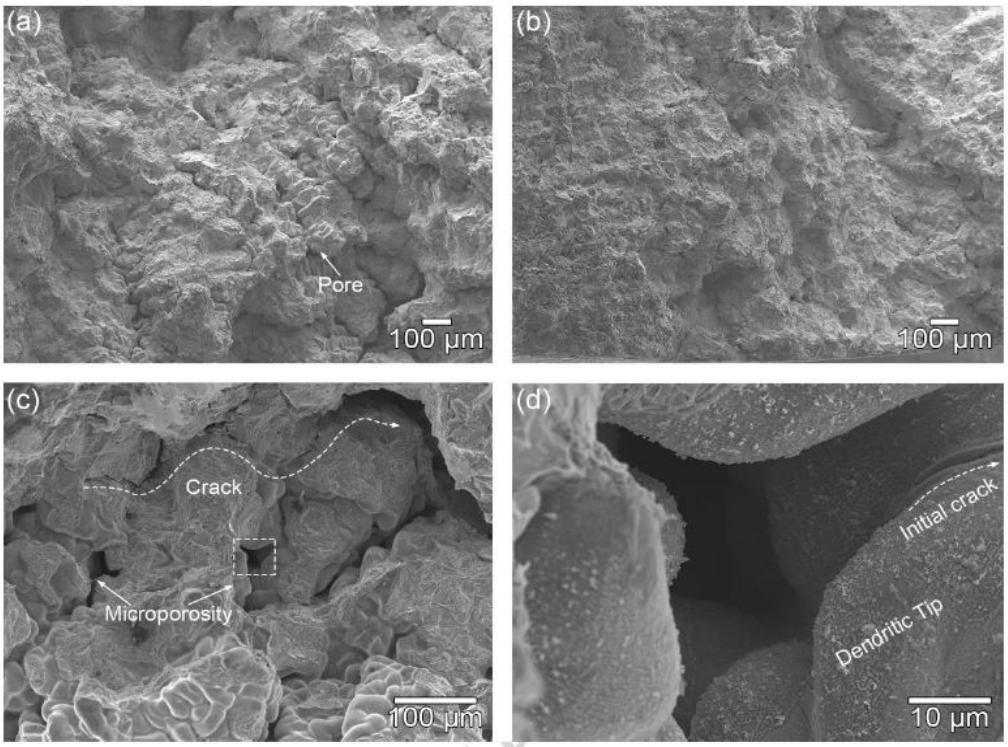

Fig.2.6: Fractography of IN-718 [62]

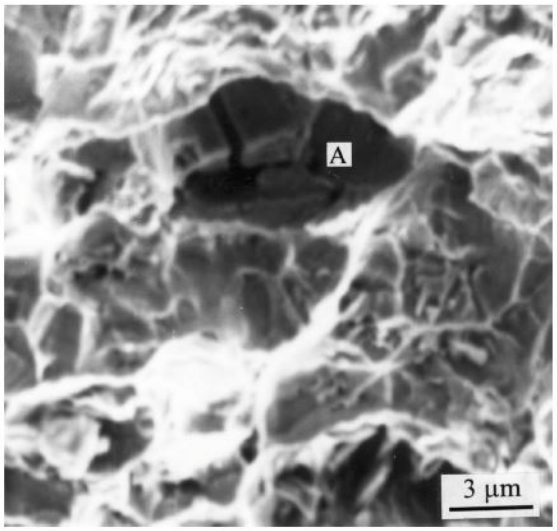

Fig.2.7: Freshly fractured carbide/matrix surface [61]

G. Appa Rao, M. Srinivas and D. S. Sarma [64] found that fracture started due to void coalescence and considerable stretching of material and fracture process may be transgranular (Fig2.8a) or intergranular (Fig2.8b) depends upon phases and microstructure of IN-718 depends upon heat treatment process.

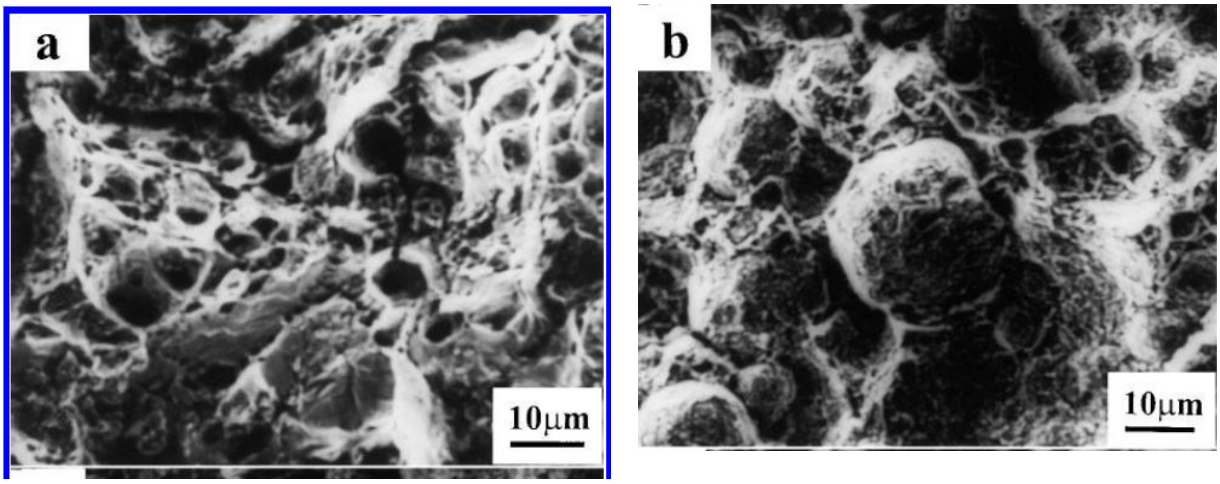

Fig 2.8: (a) HIP+1270°C/1 h/WQ and tested at room temperature; (b) HIP+955°C/1 h/WQ and aged and tested at room temperature [54]

CHAPTER 3
EXPERIMENTAL DETAILS

Chapter 3

Experimental Details

3.1 Sample Preparation

Sample for tensile test, fracture test and microstructure characterisation were prepared from forged IN-718 round bar. Chemical composition (in wt %) of the material is: Ni 52.4, Cr 17.5, Fe 19.3, Mo 2.7, Ti 0.77, Nb 5.0, Co 0.32, Mn 0.30, Cu .26, Al 0.21, C 0.08 and Si 0.21. Three sets of specimen were prepared. First set of samples consisted of five block samples, labelled M0, M1, M2, M3, M4, STD and Mar. Where M0 was solution annealed. M1 to M4 were different time aged sample, STD for standard heat treatment and Mar stand for as received sample. The second set of specimens contained 15 number of M12 round bar tensile specimens following ASTM E8M. Third group was 5 half compact tension (CT) specimens following ASTM E1820 to perform J tests at room temperature. Dimension of these specimen were given in Figure 3.1, and Figure 3.2 respectively.

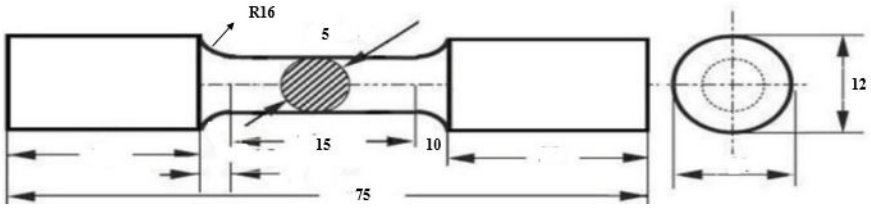

Fig.3.1: Schematic diagram of the tensile specimen. All dimensions are in mm.

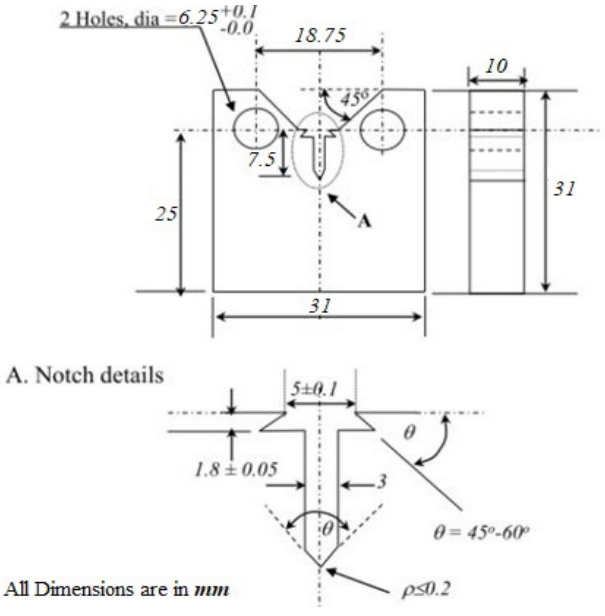

Fig.3.2: Schematic diagram of the half (0.5) CT specimen.

3.2 Heat treatment cycle

Samples were heat treated in a controlled manner at different temperatures to provide different microstructure and mechanical properties of IN-718. Heat treatments were

conducted in Carbolite CWF 1300 furnace. The heat treatment cycle used for In-718 was solution annealing at 980°C for 1 hour and then water quenched to room temperature. Further solution annealed (SA) specimens were aged by giving two step ageing treatments as shown in Fig.3.3, to form new intermetallic precipitates and various phases depending on the time and temperature of ageing. There were five sets of samples. Every set consisted of 1 block specimen, 3 tensile specimens and 1 half CT specimen. There were five types of aging treatments used for the block specimen and four types of aging cycle were used for the tensile and half CT specimens to correlate mechanical properties and microstructures. Table 3.1 showed the test matrix and sample designations. Figure 3.3 showed the schematic diagram of the heat treatment schedule. Double aging heating was intended to precipitate the different sizes/shapes of fine γ' and γ''.

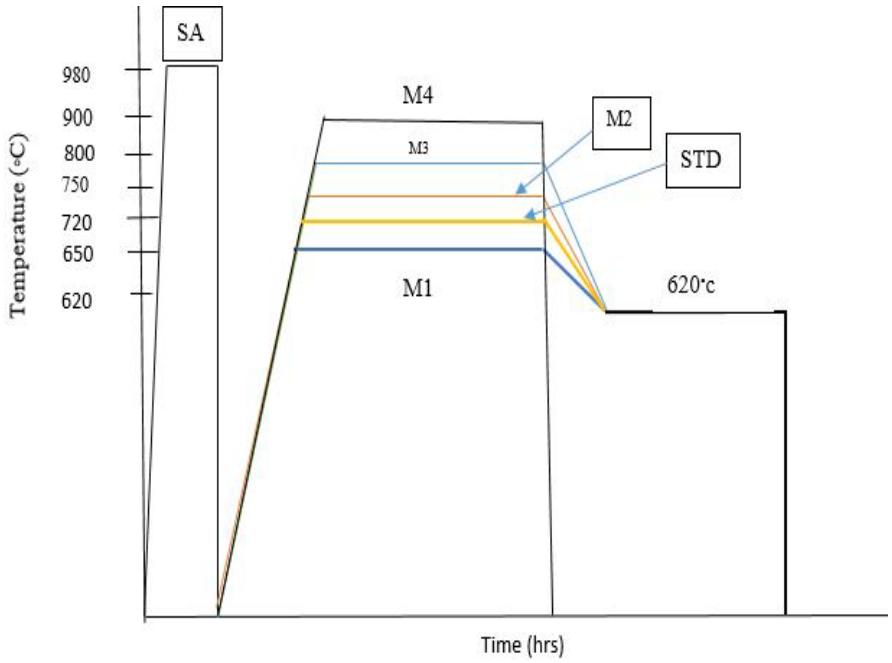

Fig.3.3: Schematic diagram of the heat treatment cycles used in the present study.

3.3 Microstructural characterisation

Metallographic specimens were prepared following standard metallographic procedure. Specimens were etched with chemical solution called Glyceregia. Glyceregia is a chemical solution of HCl, HNO_3 and Glycerol in 3:1:1 ratio. Microstructures were characterised with the help of optical microscope and scanning electron microscope (SEM). Grain size measurements were carried out using the intercept method according to ASTM: E562 with the help Image J software. EDS measurement was also carried out using SEM. The area fraction of the different particles was determined using the ASTM: E562 with the help of the Image J software. To have statistically representative results, at least 6 micrographs were considered for grain size measurement and the characterization of different particles.

Table 3.1 Test Matrix and Sample designation for tensile specimen and half CT specimen

SI NO	Sample Designation	Aging Cycle	Testing Temperature (°C)	Expected Phase
1	M1	SA + 650°C (75hrs) + 620°C (8hrs)	RT	γ
2	M1a		650	
3	M1b		650	
4	M2	SA + 750°C (75hrs) + 620°C (8hrs)	RT	γ'+ γ"
5	M2a		650	
6	M2b		650	
7	M3	SA + 800°C (75hrs) + 620°C (8hrs)	RT	γ'+ γ"+ δ
8	M3a		650	
9	M3b		650	
10	M4	SA + 900°C (75hrs)	RT	δ
11	M4a		650	
12	M4b		650	
13	STD	SA+ 720°C(8hrs)+ 620°C (8hrs)	RT	γ'+ γ"
14	STD		650	
15	STD		650	

3.4 Mechanical testing

3.4.1 Micro Hardness

Hardness test was done by Vickers hardness test machine using the load of 30 kgf and dwell period is 10 seconds. Five measurements were taken in each sample.

3.4.2 Tensile test

Fifteen heat treated samples were tested at room temperature and high temperature (650°C) by Servo-Electric Instron 8862 (shown in Figure 3.4) with 100 kN load capacity using a strain rate of 0.001 per sec.

3.4.3 Fractography

Fracture surface of all specimens were preserved in desiccator. Most of the fractographic images were taken from central region of cup type fracture surface.

3.5 Fracture

3.5.1 Specimen Precracking

All the specimens were precracked using Servo-Hydraulic INSTRON 8501 with constant Stress intensity factor (ΔK) of 21Mpa√m with frequency 20Hz. DADN software was used to measure the crack online following elastic unloading compliance method. Specimen loaded under the actuator was connected with a COD gauge. Figure 3.5 showed the specimen loaded under the actuator for pre-cracking.

Fig. 3.4: Set up for high temperature tensile test.

Fig. 3.5: Set-up used for pre-cracking of the specimens.

3.5.2 J-Integral test

All the pre-cracked specimens were then tested at room temperature for J- integral on same machine which was used for tensile tests. Epsilon made Crack Opening Displacement (COD) gauge (was of 5 mm gauge length and 12 mm travel shown in Figure.3.6) was used to measure the COD.

Fig.3.6: Half CT specimen during the room temperature J-test is in progress.

Load – LLD curves were obtained from the experimental data and then J-R curves were computed by using J-Calculation procedure described in Chapter-2. J-integral test has been carried out considering the waveform presented in Figure 3.7. The whole load displacement plot cycle consists of repeated loading relaxation and unloading cycle respectively.

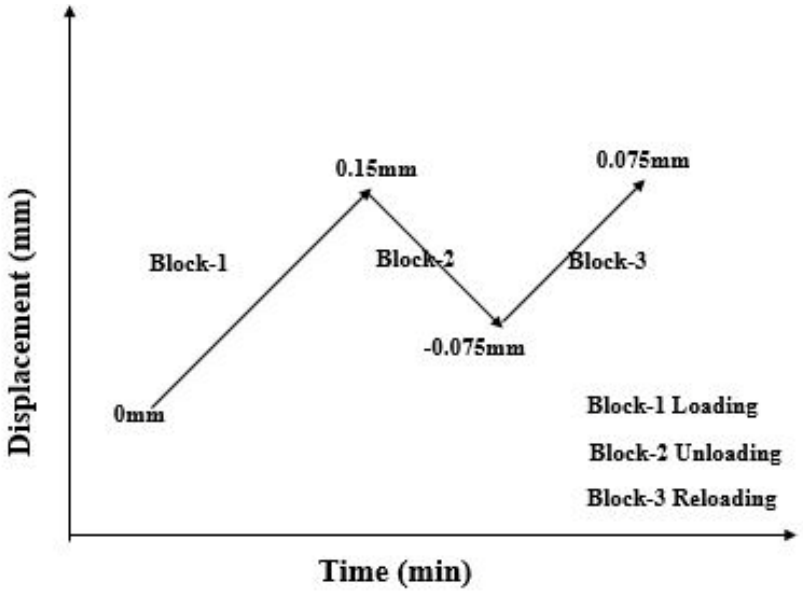

Fig. 3.7 Waveform used to perform J-Test.

CHAPTER 4
RESULTS AND DISCUSSION

Chapter 4

Results and Discussion

4. Microstructure

4.1 Optical Microstructure analysis

Fig.4. 2 (a-g) shows the microstructures of the block specimen. The microstructure consists of polyhedral grain with annealing twins. The grain size was measured following ASTM E112 standard and linear intercept method. The average grain size of the as received sample is 20μm±4. The average grain size of the as received and the heat treated sample is presented in the Fig. 4.1.

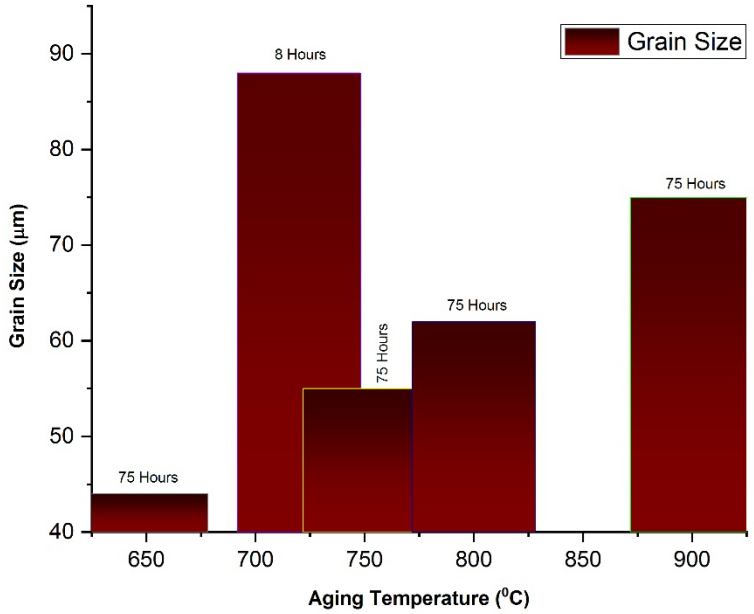

Fig. 4.1: Effect of aging treatment on the grain size

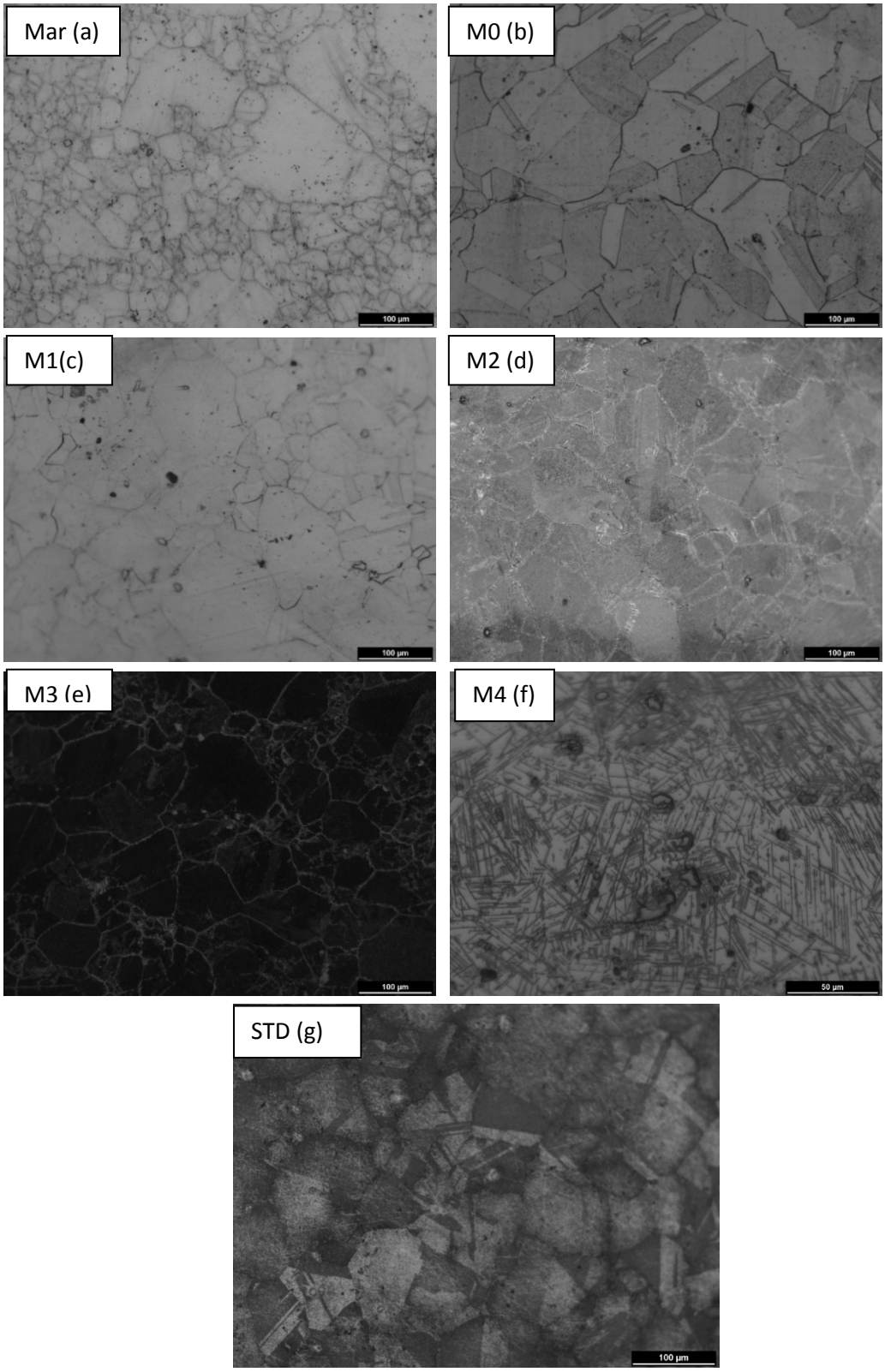

Fig.4.2: Microstructures of the specimens

4.2 Scanning Electron Microscope analysis

Carbides are equally distributed along the grain boundaries and within the grains (Fig 4.3). NbC carbides are present the grain boundaries. After solution annealing treatment at 980°C for 1hr, most of the carbides were dissolved in the solution. Some blocky precipitates could be seen at grain boundaries as well as within the matrix (Figure 4.4. NbC and (Cr, Fe, $Mo)_{23}C_6$ carbides are present at the grain boundaries and Fe_3Mo_3C, Fe_3Nb_3C and Nb_3Co_3C carbide are formed in the matrix. Microstructure and EDS mapping of the sample M0 (Fig.4.4) shows that γ phase form in the Ni matrix.

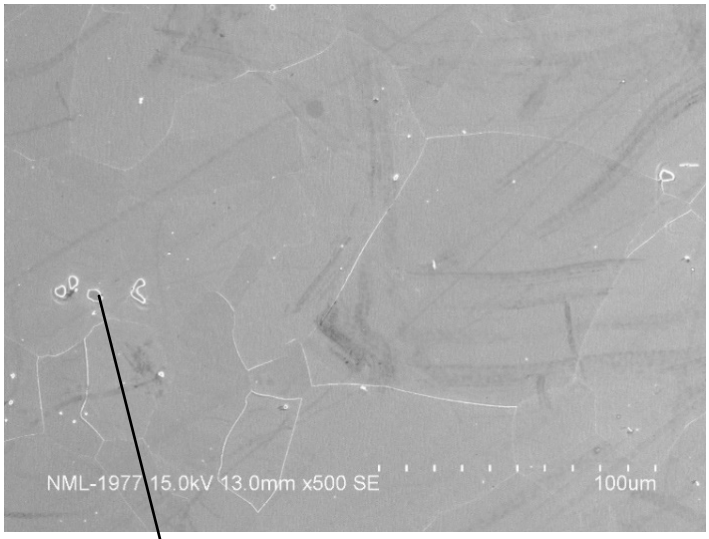

Fig. 4.3 SEM image of the as-received Inconel 718

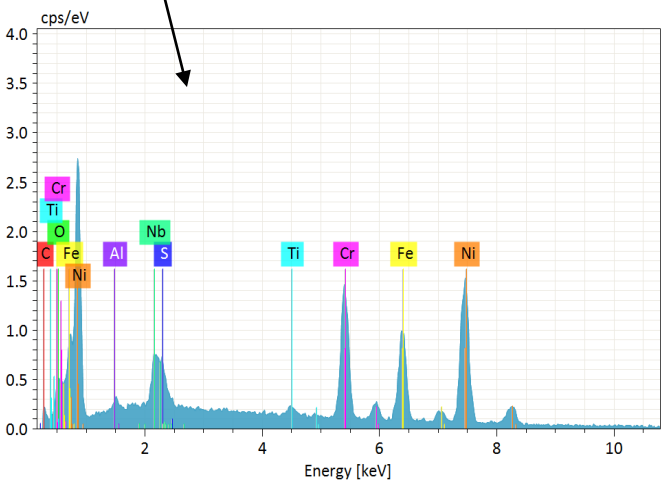

EDS of as-received Inconel 718

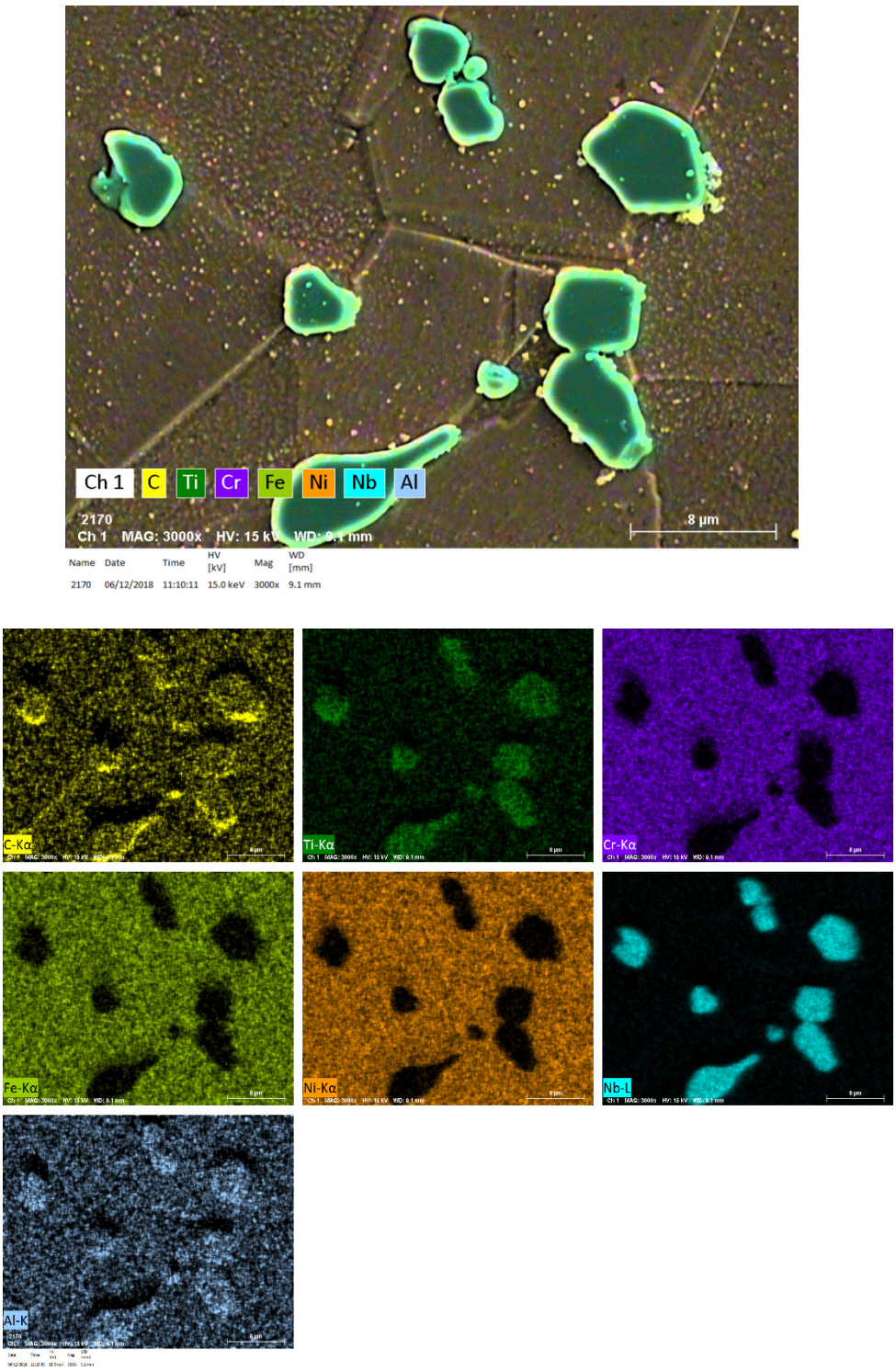

Fig.4.4: EDS mapping of the M0 specimen.

Sample M1 show (Figure 4.5) slightly different microstructure, but M0 and M1 have same phase of γ that's concluded from EDS and SEM.

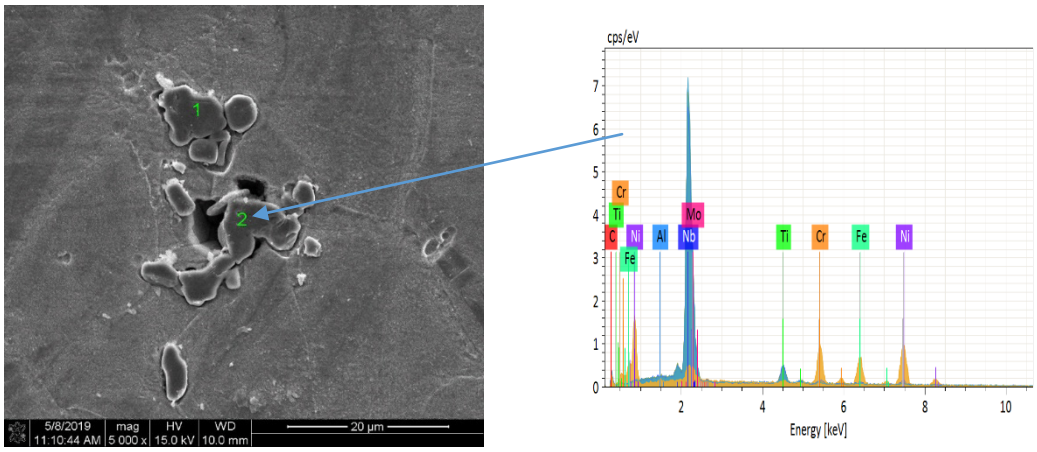

Fig.4.5: SEM image of M1 specimen

Twinning is always recognized as one of the plastic deformation mechanisms of Inconel 718 and could be seen almost everywhere before and after heat treatments (Figure 4.6). The presence of extensive twins is observed in the samples heat-treated at lower temperatures (700-775◦C), which act as nucleation sites for recrystallization.

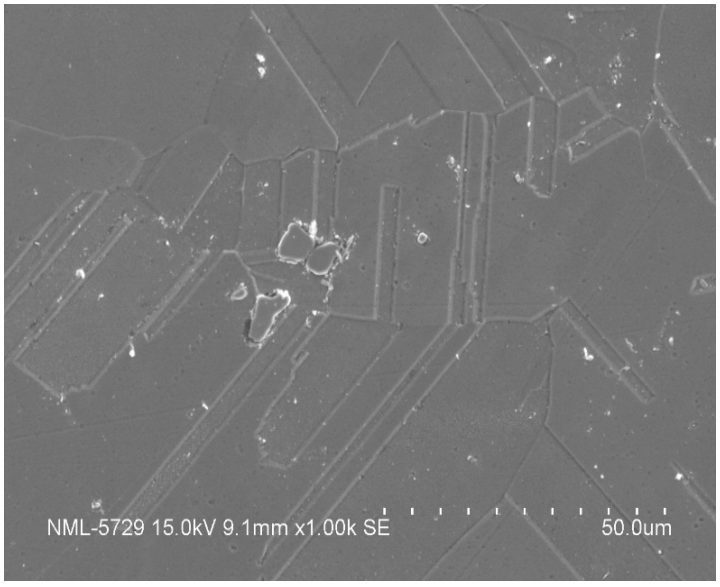

Fig.4.6: Twinning in the sample M0

.

SEM and EDS characterisation shows (figure.4.7) that sample M2 have both γ' ($Ni_3(Al, Ti)$) and γ'' (Ni_3Nb), $Cr_{21}Mo_2C_6$ and $Mo_3(Ni, Co)_3$ precipitates.

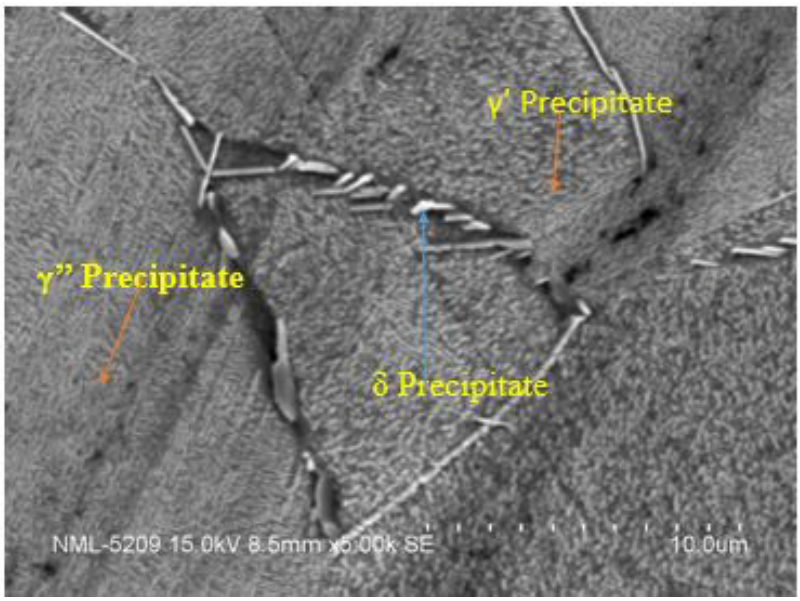

Fig.4.7: Precipitates present in the sample M2

The δ, γ' and γ'' precipitates in the sample M3 is shown in the figure.4.8. The composition analysis of the δ and γ'' and carbide precipitates are also shown in Figure 4.8.

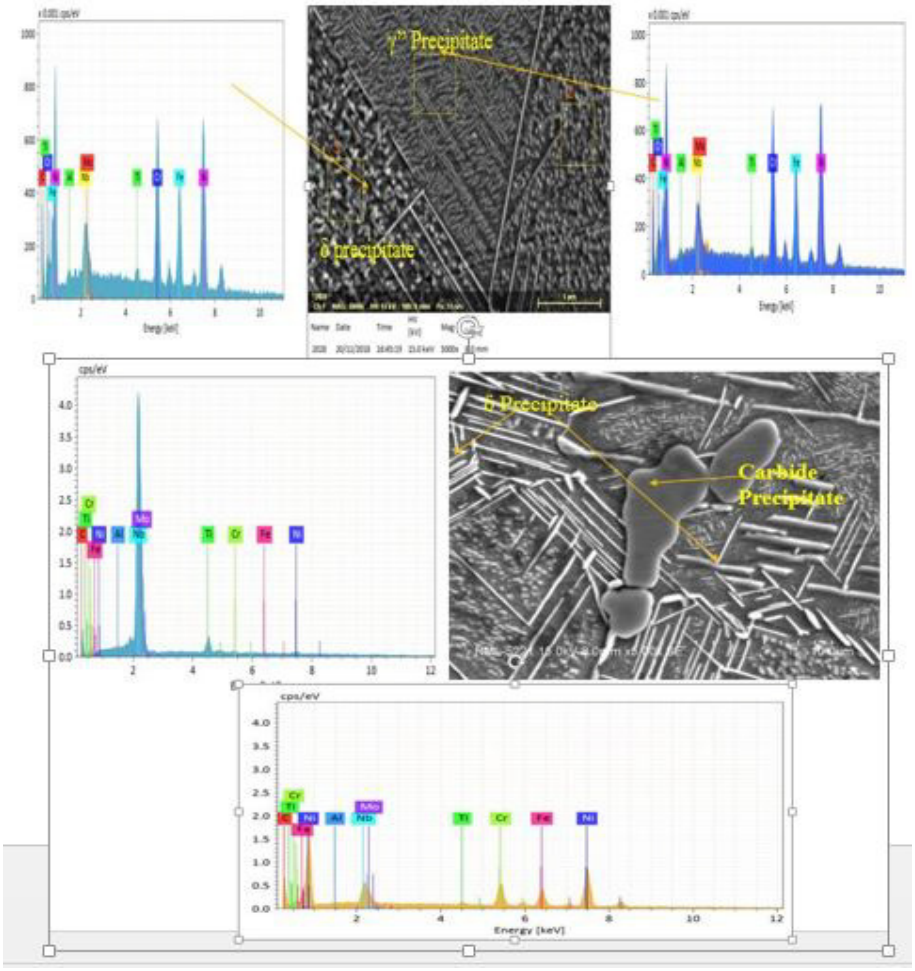

Fig.4.8: γ', γ'', δ and carbide precipitation of sample M3 and Table show EDS.

The second type of precipitates are rich in Nb and Ti with globular or needle shape lying perpendicular to polished surface (Figure 4.9a) are identified as δ phase. In some regions, one variant appeared to have enveloped another variant probably during its growth. δ phase grows through the formation of an intermittent γ'' phase (Figure 4.8b). The δ precipitates have also plate shaped morphology (Figur 4.8(c)). Further all sample types of precipitate and variety are given in table 4.1 which has been concluded by EDS. Precipitate

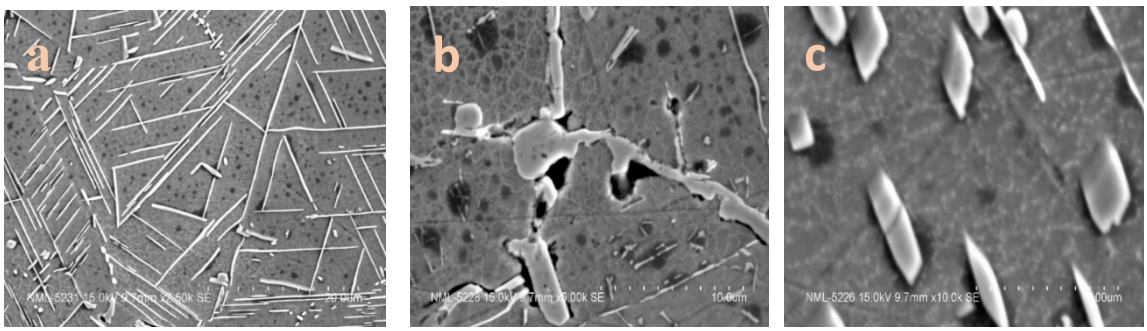

Fig.4.9: (a) δ precipitates with needle shaped (b) one variant appeared to have enveloped another variant (c) δ precipitates with plate morphology

Table 4.1 Types of precipitate and composition obtained with heat treatment

Sample Designation	Aging Cycle	Obtained Phase	Composition
M0	980°C for 1 hr	**γ**	NbC, (Cr, Fe, $M_{23}C_6$
M1	SA + 650°C (75hrs) + 620°C (8hrs)	**γ' + γ''**	Fe_3Mo_3C, Fe_3Nb_3C Nb_3Co_3C
M2	SA + 750°C (75hrs) + 620°C (8hrs)	**γ' + γ'' + δ**	$(Ni_3(Al, Ti))$ (Ni_3Nb), $Cr_{21}Mo_2C_6$ $Mo_3(Ni, Co)_3$
M3	SA + 800°C (75hrs) + 620°C (8hrs)	**γ' + γ'' +δ**	$(Ni_3(Al, Ti))$ (Ni_3Nb), $Cr_{21}Mo_2C_6$ $Mo_3(Ni, Co)_3$.
M4	SA + 900(75hrs)	**δ**	Ni_3Nb

4.3 Hardness test

The variation of hardness with the aging temperature is presented in the Fig 4.10. Hardness of as received sample is 327.5 HV. Whereas hardness after solution annealing is decreased very drastically (168.37 HV). After aging hardness increases. Sample M1 have highest hardness then after aging the hardness value decreases. That suggests γ' precipitate has highest influence on the hardness.

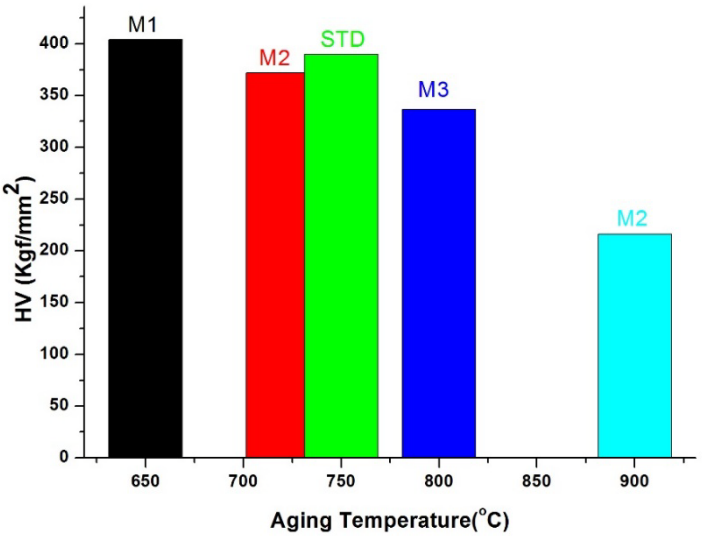

Fig.4.10. Effect of heat treatment on the hardness

4.4 Tensile result

Tensile test result of the various heat treated sample tested at RT and HT (650˚C) are given below in Table 4.2.

Table 4.2 Variation of tensile properties

Sample	**Temp (^{0}C)**	**YS (MPa)**	**UTS (MPa)**	**Strain-Hardening Exponent (n)**	**Strength Coefficient (K)**	**Reduced Area (%)**	**Elonga-tion(%)**
M1	RT	821	1157	0.19	1837.77	16.79	42
M1a	650˚C	844	1003	0.09	1379.71	25.76	17
M1b	650˚C	919	1017	0.06	1296.46	20.41	12
M2	RT	821	1232	0.17	1938.77	39.76	31
M2a	650˚C	757	977	0.1	1446.64	39.76	30
M2b	650˚C	729	854	0.1	1399.65	36.24	28
M3	RT	722	1188	0.21	1994.54	31.59	32
M3a	650˚C	821	1157	0.17	1493.14	41.21	33
M3b	650˚C	644	959	0.17	1582.6722	36.69	28
M4	RT	452	897	0.29	1646.85	40.38	41
M4a	650˚C	467	717	0.18	7.04223	39.75	25
M4b	650˚C	549	769	0.14	1142.87	31.99	30
STD1RT	RT	1029	1302	0.13	1926.38	28.85	37
STD1HT	650˚C	850	985	0.07	1299.98	14.67	15
STD2HT	650˚C	924	1068	0.08	1433.53	6.34	14

4.4.1 Effect of heat treatment on the tensile strength

Standard heat treated sample have highest YS and UTS among all. The tensile strength at elevated temperature was slightly deteriorated for almost all the samples. YS of sample M1 and M4 at high temperature have greater value than YS at room temperature. This happens due to transformation of carbides. Ductility of sample M1 and STD decreases drastically at high temperature. M4 sample have lowest value of YS and UTS among all specimen due to formation of the δ phase. M2 shows the optimum combination of strength and ductility at

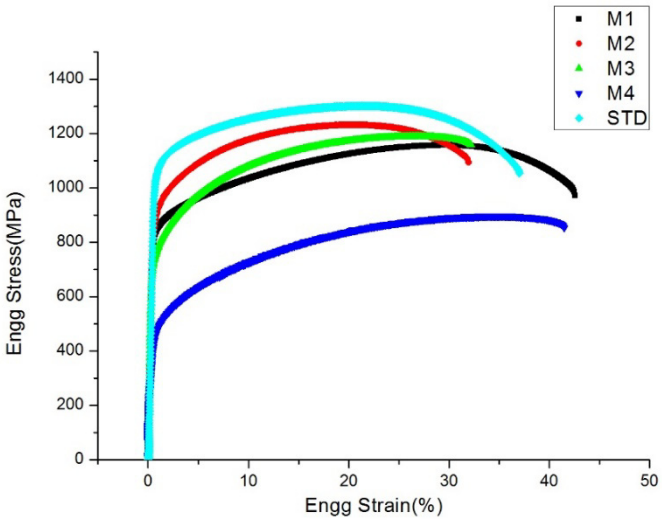

Fig.4.11: Tensile behaviour of various samples at room temperature

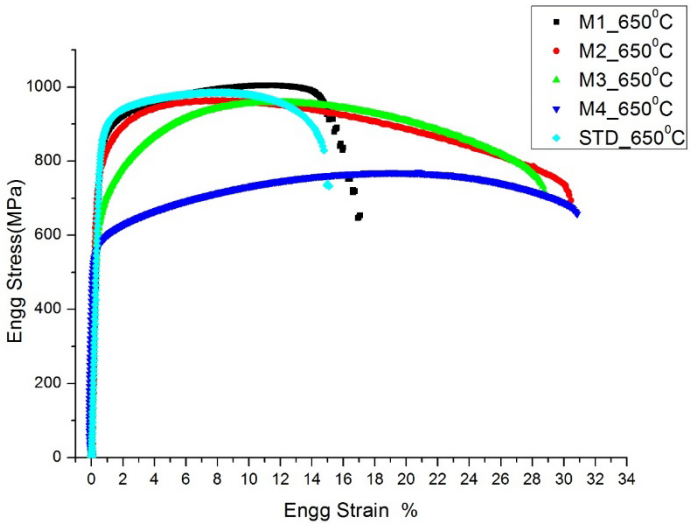

Fig. 4.12: Tensile behaviour at 650°C temperature

4.4.2 Effect of Aging on the yield and tensile strength

Aging process has been done in two steps. In first step, temperature was different in every sample. However the aging time was similar except for the STD sample (720°C and 8Hrs). Hence varying temperature in the first step contributes to the difference in strength (Fig 4.13 and 4.14). The different aging temperatures result in the gradient in the precipitate population (fig 4.13 and 4.14). Aging produced maximum effect between 650°C and 750°C due to high area fraction of γ' and γ''. After 750°C to 900°C delta phase start to form.

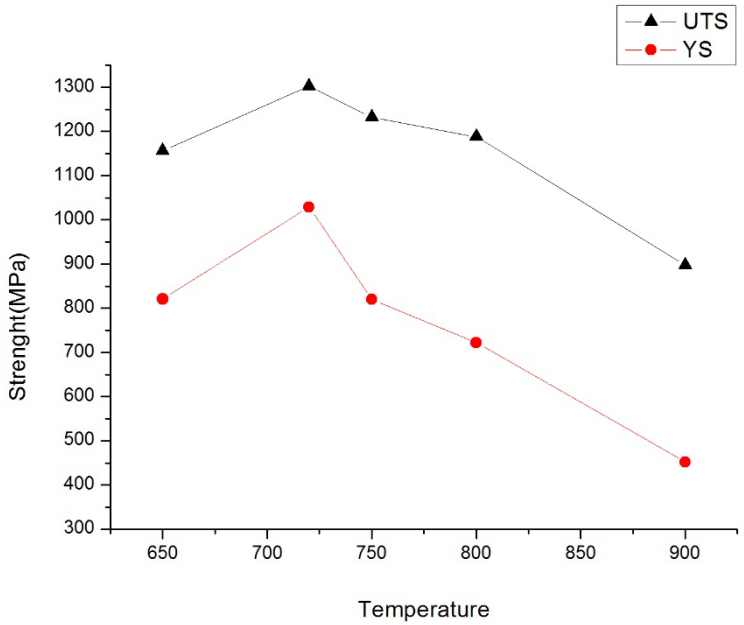

Fig 4.13: Aging effect on the tensile strength at room temperature

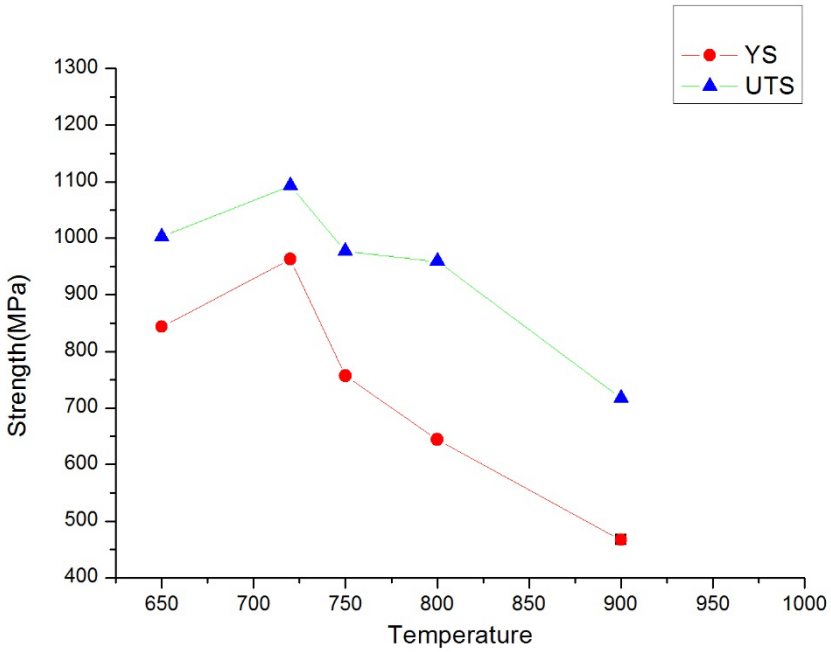

Fig.4.14: Aging effect on the tensile strength at 650°C

4.4.3 Effect of Precipitation number density on strength at room temperature and high temperature test

Result of precipitate number density with strength is presented in the Figure. 4.15 and Figure 4.16 The higher the precipitate density the higher will be the strength (UTS) at room temperature as well as at 650^{o}C. γ'' is smallest in size among all precipitate and δ is largest [70].

Table 4.3 Precipitate number density

Sample	Precipitate Density No of Precipitate/Area(mm^2)
M1	0.22171
M2	6.18143
M3	3.42333
M4	0.0098
STD	8.2816

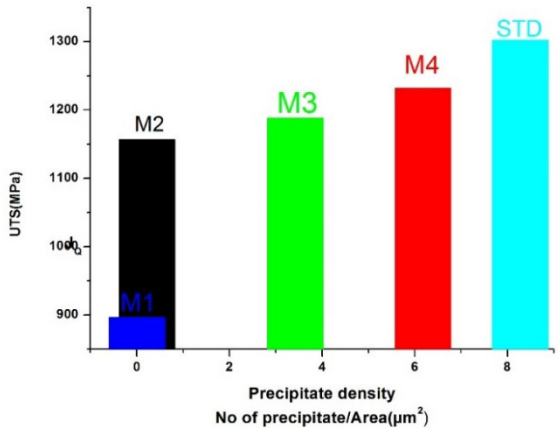

Fig.4.15: Effect of precipitate number density on UTS at room temperature

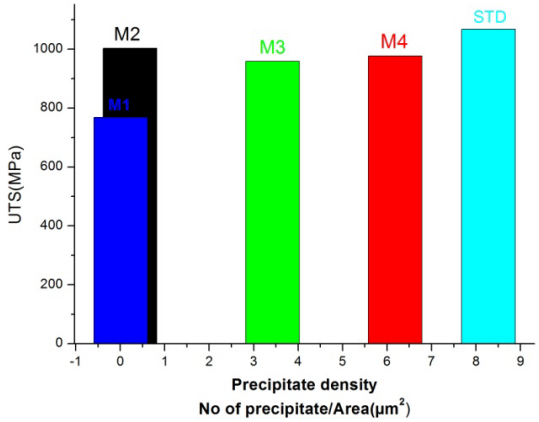

Fig.4.16: Effect of precipitate number density on UTS at 650°C

4.4.4 Effect of Aging on ductility at room temperature and high temperature test

The variation of elongation with the aging temperature is shown in the Figure 4.17 and Figure 4.18. Every sample of at room temperature have high value of elongation approx 30 to 40% .M1 and M4 have higher elongation than standard specimen. But ductility of M1 and STD sample decrease drastically at 650^{o} C due to very high rate of coalescence of micro-voids at 650^{o} C.

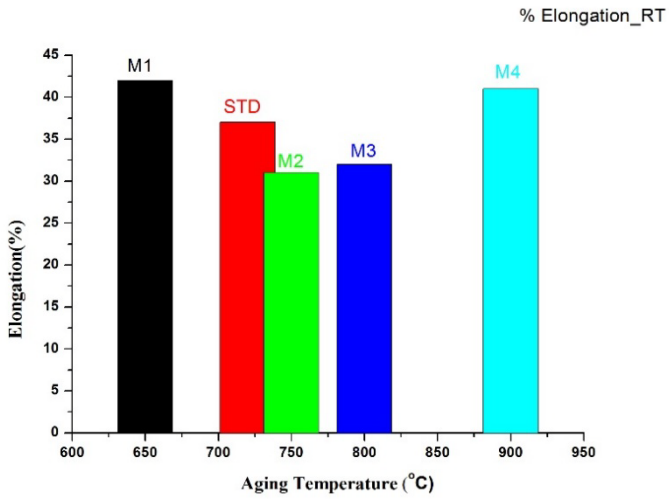

Fig.4.17: Effect of Aging on the tensile elongation at room temperature.

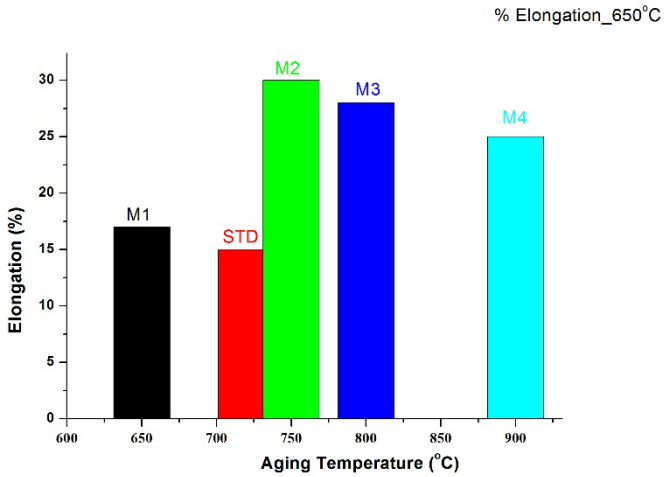

Fig4.18: Effect of Aging on the tensile elongation at 650^{o}C temperature.

4.5 Fractographic features

The fracture surfaces of the aged specimens were examined in SEM (Figure 4.19). A dimpled rupture which is characterized by cup-and-cone-like depression was observed for all specimens in all the condition of the tests. It can be observed that the major crack originates at the centre of the specimen along the loading axis which has propagated radially outwards before final fracture in a cup-and-cone shape. The shear lip zones are observed at the circumference of the fractured surfaces at both temperatures. The voids are observed which further confirms ductile failure as the mechanism of fracture.

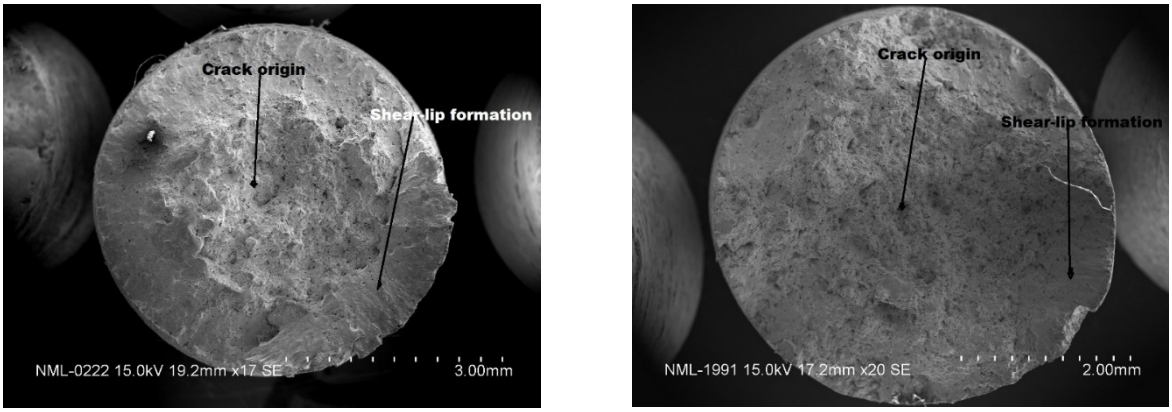

Fig 4.19: Fracture mode in tensile tests at (a) room temperature and (b) 650˚C

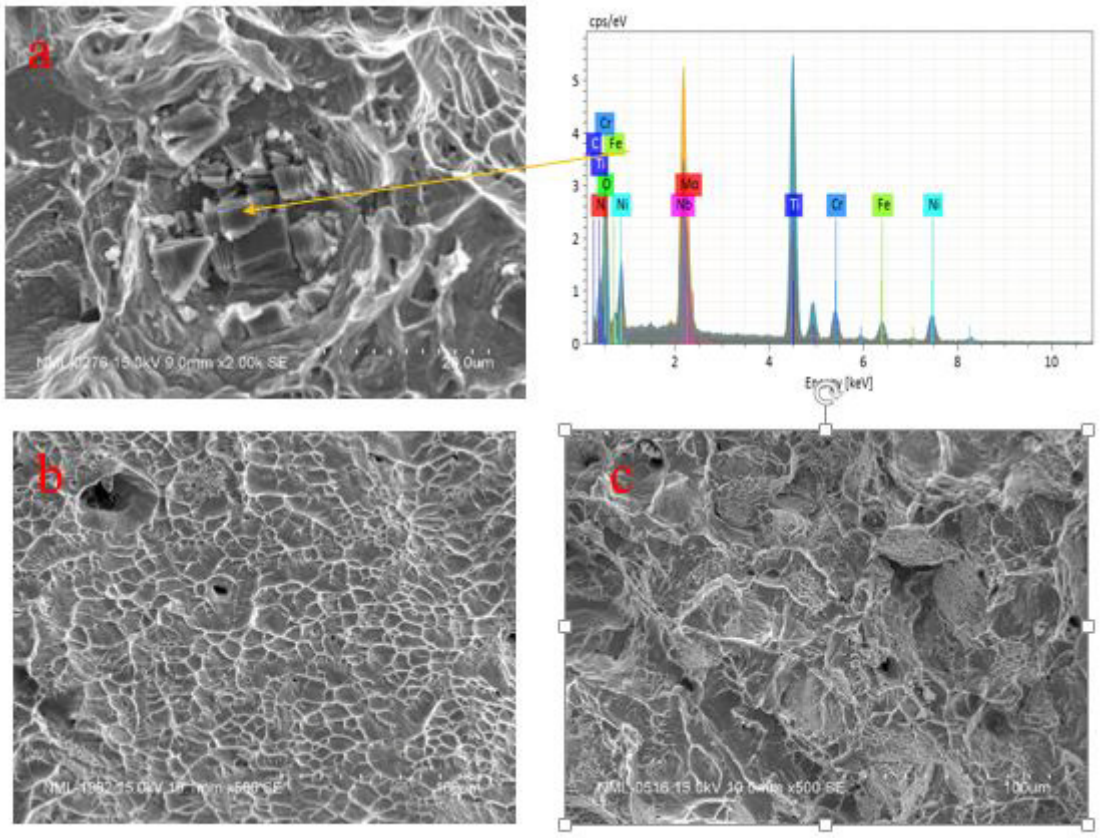

Fig.4.20: (a) Crack initiation point during tensile test Fractographic image of sample M1 (b) at room temperature, (c) At 650˚C

The wide and deep void in fig 4.14 near the centre of the micrograph contains a carbide. These carbides are apparently the major source for crack nucleation These carbide are weaker due to the presence of impurity like nitrogen and oxygen. There are stress concentration at these carbides due to slip.

4.6 Fracture Experimental Results

Result obtained from the tensile tests shows that ductile mode of fracture occur in IN-718. So fracture cannot be estimated by LEFM analysis. So the governing parameter, initiation fracture toughness, J_{Ic} was determined through EPFM analysis for all the materials at room temperature. Fig. 4.21 shows the J-R behaviour of the materials at room temperature with various heat treatment process. It was observed that the STD materials have shown the highest J_{Ic} values compared to the other remaining samples. J_{Ic} for all samples are given in table 4.4. and Figure 4.22.

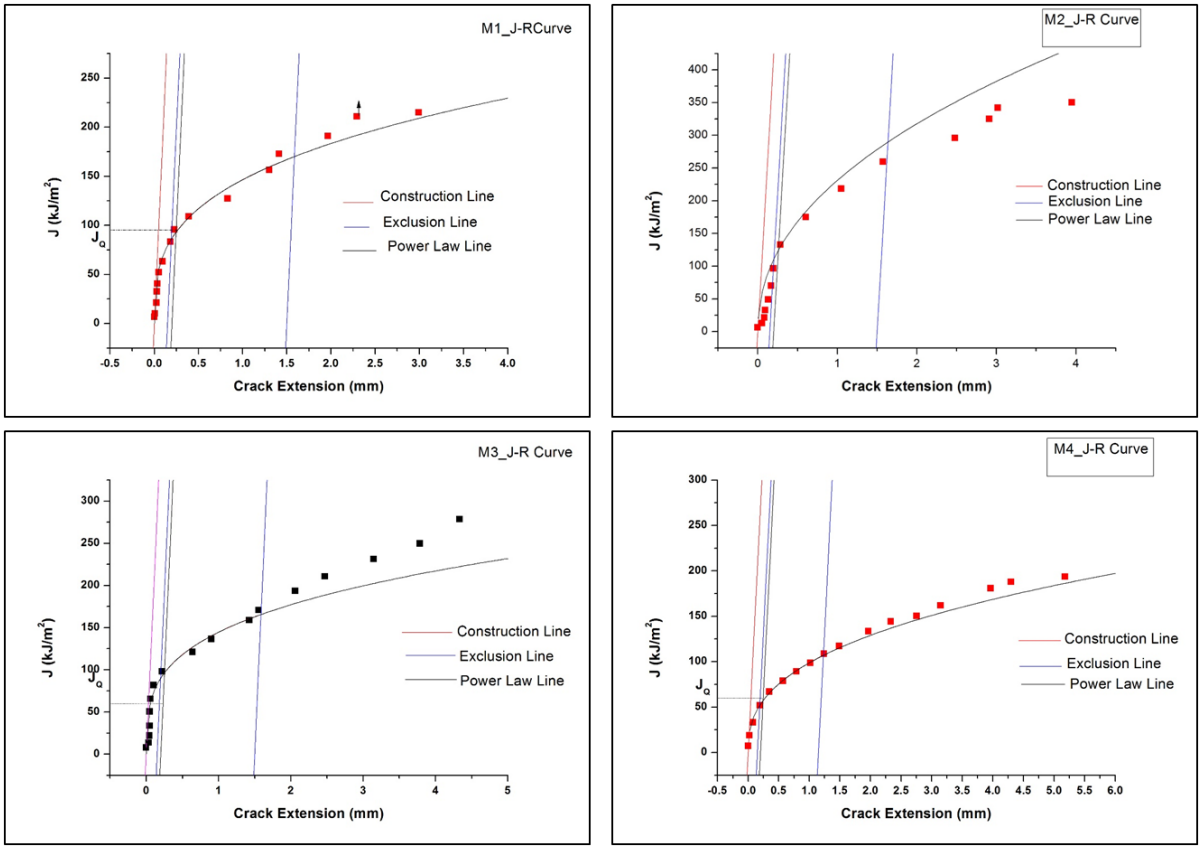

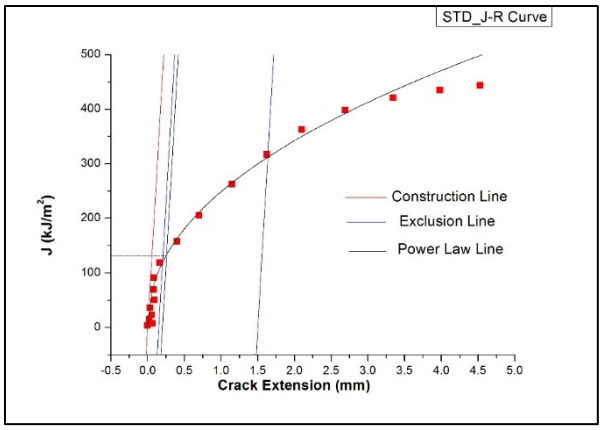

Fig. 4.21: J-R curve of M1, M2, M3, M4 and STD material obtained through experimental analysis

Table 4.4 Initiation fracture toughness (J_{Ic}) values of SHT & MHT IN-718 in room temperature

Sample Designation	J_{Ic} (kJ/m^2)	Δa_{min} (0.15mm offset line) (mm)
M1	92.63	0.19445
M2	122.818	0.201836
M3	96.39	0.1969
M4	57.0679	0.1876
STD	133.199	0.1985

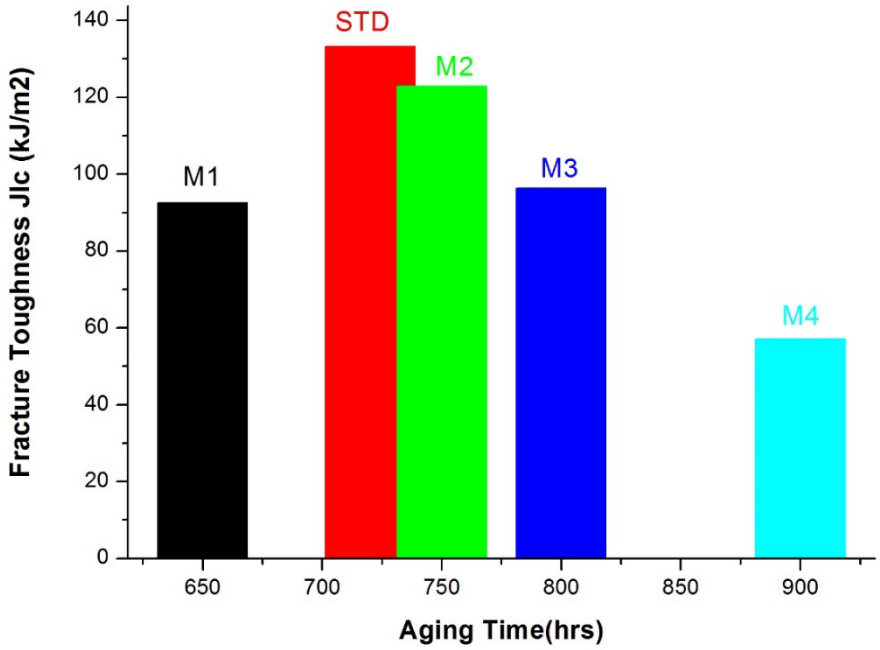

Fig.4.22: Effect of aging on the tensile elongation at room temperature

CHAPTER 5

CONCLUSIONS & FUTURE WORK PLAN

Chapter 5

Conclusions

Based on the results following conclusions can be made:

- Various types of phases like γ' γ'' and δ can be obtained and the amount of these phases can controlled by changing temperature range during heat treatment.
- γ'' phase has most influence on mechanical property and δ phase has least influence.
- Maximum γ'' is obtained by SHT process.
- Standard heat treated sample have higher value of YS and UTS at both room temperature and at 650^{o}C.
- The tensile strength at 650^{o}C was slightly deteriorated for almost all the specimens.
- Sample M1 and M4 have higher YS at elevated temperature than YS at room temperature.
- SHT provided the high initiation fracture toughness, $J_I c$ value at room temperature.

Future Work Plan

- TEM and EBSD can be used to characterize the different phases present in heat treated materials.
- Tensile properties at different strain rate can be done on this material to check strain rate sensitivity.
- Effect of Laves and Eta phase on mechanical properties can be checked by producing these phases upon taking different sets of aging time and in IN-718.
- Fatigue property can be checked at room temperature and at elevated temperature.

References

1. Akca, E. and A. Gürsel, *A review on superalloys and IN718 Nickel-based INCONEL superalloy.* Periodicals of Engineering and Natural Sciences (PEN), 2015. **3**(1).
2. Sabol, G. and R. Stickler, *Microstructure of Nickel-Based Superalloys.* physica status solidi (b), 1969. **35**(1): p. 11-52.
3. Donachie, M.J. and S.J. Donachie, *Superalloys: a technical guide*2002: ASM international.
4. Wilcox, B., et al., *The Superalloys.* 1972.
5. Sims, C.T., N.S. Stoloff, and W.C. Hagel, *superalloys II*1987: Wiley New York.
6. Eiselstein, H., *Metallurgy of a columbium-hardened Nickel-chromium-iron alloy*, in *Advances in the technology of stainless steels and related alloys*1965, ASTM International.
7. Bradley, E., *Superalloys: a technical guide', 1988.* Metals Park, OH, ASM International.
8. Whitmore, L., et al., *The microstructure of heat-treated Nickel-based superalloy 718Plus.* Materials Science and Engineering: A, 2014. **610**: p. 39-45.
9. Mignanelli, P.M., et al., *Gamma-gamma prime-gamma double prime dual-superlattice superalloys.* Scripta Materialia, 2017. **136**: p. 136-140.
10. Reed, R.C., *The superalloys: fundamentals and applications*2008: Cambridge university press.
11. Sims, C.T. and W.C. Hagel, *The Superalloys-vital high temperature gas turbine materials for aerospace and industrial power*1972: John Wiley & Sons.
12. Ghosh, S., S. Yadav, and G. Das, *Study of standard heat treatment on mechanical properties of Inconel 718 using ball indentation technique.* Materials letters, 2008. **62**(17-18): p. 2619-2622.
13. Slama, C., C. Servant, and G. Cizeron, *Aging of the Inconel 718 alloy between 500 and 750 C.* Journal of materials research, 1997. **12**(9): p. 2298-2316.
14. Thomas, A., et al., *High temperature deformation of Inconel 718.* Journal of Materials Processing Technology, 2006. **177**(1-3): p. 469-472.
15. Ardell, A. and R. Nicholson, *The coarsening of γ'in Ni-Al alloys.* Journal of Physics and Chemistry of Solids, 1966. **27**(11-12): p. 1793-1794.
16. Lifshitz, I.M. and V.V. Slyozov, *The kinetics of precipitation from supersaturated solid solutions.* Journal of Physics and Chemistry of Solids, 1961. **19**(1-2): p. 35-50.
17. Wagner, C., *Theorie dealtering von Niederschlagen durch uml7pt" ösen Z.* Elektrochem, 1961. **65**: p. 581.
18. Xie, X.S., et al. *High temperature structure stability study on Nb-containing Nickel-base superalloys*. in *Materials science forum*. 2007. Trans Tech Publ.
19. Vishwakarma, K., N. Richards, and M. Chaturvedi, *Microstructural analysis of fusion and heat affected zones in electron beam welded ALLVAC® 718PLUS™ superalloy.* Materials Science and Engineering: A, 2008. **480**(1-2): p. 517-528.
20. Vishwakarma, K. and M. Chaturvedi. *A study of HAZ microfissuring in a newly developed Allvac® 718 PLUSTM superalloy*. in *Proceedings of the International Symposium on Superalloys*. 2008.
21. Bhadeshia, H., *Recrystallisation of practical mechanically alloyed iron-base and Nickel-base superalloys.* Materials Science and Engineering: A, 1997. **223**(1-2): p. 64-77.
22. Lund, C.H., *Physical Metallurgy of Nickel-Base Superalloys*, 1961, BATTELLE MEMORIAL INST COLUMBUS OH DEFENSE METALS INFORMATION CENTER.
23. Azadian, S., L.-Y. Wei, and R. Warren, *Delta phase precipitation in Inconel 718.* Materials characterization, 2004. **53**(1): p. 7-16.
24. Wang, H., et al., *Investment Casting Solidification Simulation of Nickel-Based Superalloys: Micro Modeling Aspects.* Transactions of the American Foundrymen's Society., 1993. **101**: p. 771-779.

25. Chapman, L., *Application of high temperature DSC technique to Nickel based superalloys.* Journal of Materials Science, 2004. **39**(24): p. 7229-7236.
26. Devaux, A., et al., *Gamma double prime precipitation kinetic in Alloy 718.* Materials Science and Engineering: A, 2008. **486**(1-2): p. 117-122.
27. Kuo, C.-M., et al., *Aging effects on the microstructure and creep behavior of Inconel 718 superalloy.* Materials Science and Engineering: A, 2009. **510**: p. 289-294.
28. Sundararaman, M., P. Mukhopadhyay, and S. Banerjee, *Precipitation of the δ-Ni 3 Nb phase in two Nickel base superalloys.* Metallurgical transactions A, 1988. **19**(3): p. 453-465.
29. Kirman, I. and D. Warrington, *The precipitation of Ni 3 Nb phases in a Ni− Fe− Cr− Nb alloy.* Metallurgical Transactions, 1970. **1**(10): p. 2667-2675.
30. Kirman, I., *Precipitation in the Fe-Ni-Cr-Nb system.* J Iron Steel Inst, 1969. **207**(12): p. 1612-1618.
31. Durand-Charre, M., *The microstructure of superalloys*2017: Routledge.
32. Betteridge, W., *The nimonic alloys*1959: E. Arnold.
33. Chang, S.-H., et al., *Influences of soaking time in hot isostatic pressing on strength of inconel 718 superalloy.* Materials transactions, 2006. **47**(2): p. 426-432.
34. Lee, S.-C., et al., *Improvement in the microstructure and tensile properties of Inconel 718 superalloy by HIP treatment.* Materials transactions, 2006. **47**(11): p. 2877-2881.
35. Slama, C. and M. Abdellaoui, *Structural characterization of the aged Inconel 718.* Journal of Alloys and Compounds, 2000. **306**(1-2): p. 277-284.
36. Cozar, R. and A. Pineau, *Morphology of γ'and γ" precipitates and thermal stability of inconel 718 type alloys.* Metallurgical Transactions, 1973. **4**(1): p. 47-59.
37. Cao, W. and R. Kennedy, *THERhlAL STABILITY OF ALLOYS 718 AND ALLVAC 7 1%~~.*
38. Brooks, J. and P. Bridges, *Metallurgical stability of Inconel alloy 718.* Superalloys, 1988. **88**: p. 33-42.
39. Collier, J.P., et al., *The effect of varying AI, Ti, and Nb content on the phase stability of INCONEL 718.* Metallurgical transactions A, 1988. **19**(7): p. 1657-1666.
40. Li, R., et al., *Isolation and determination for δ, γ' and γ "phases in Inconel 718 alloy.* Scripta Materialia, 2002. **46**(9): p. 635-638.
41. Chang, K.-M. and A.H. Nahm, *Rene 220: 100 deg F(38 deg C) Improvement Over Alloy 718.* Superalloy 718: Metallurgy and Applications, 1989: p. 631-646.
42. Huang, Y. and T.G. Langdon, *The evolution of delta-phase in a superplastic Inconel 718 alloy.* Journal of Materials Science, 2007. **42**(2): p. 421-427.
43. Beaubois, V., et al., *Short term precipitation kinetics of delta phase in strain free Inconel* 718 alloy.* Materials Science and technology, 2004. **20**(8): p. 1019-1026.
44. Dehmas, M., et al., *TEM study of high-temperature precipitation of delta phase in Inconel 718 alloy.* Advances in materials science and engineering, 2011. **2011**.
45. Cao, W. and R. Kennedy, *Role of chemistry in 718-type alloys–Allvac® 718Plus™ alloy development.* Superalloys 2004, 2004: p. 91-99.
46. Collier, J., A. Selius, and J. Tien, *On developing a microstructurally and thermally stable iron-Nickel base superalloy.* J. P. Collier, A. O. Selius, J. K. Tien, Superalloys 1988, 1988: p. 43-52.
47. Manriquez, J.A., et al., *The high temperature stability of IN718 derivative alloys*, 1992, TMS. p. 507-516.
48. Guo, E., F. Xu, and E. Loria, *Improving thermal stability of alloy 718 via small modifications in composition.* Superalloy 718– Metallurgy and Applications, 1989: p. 567-576.
49. Xu, F., E. Guo, and E. Loria, *Thermal stability of modified 718 alloys aged for 2000 hours at 700 deg C.* Superalloys 718, 625, 706 and Various Derivatives, 1997: p. 503-509.
50. Tien, J., J.P. Collier, and G. Vignoul, *The role of Niobium and other refractory elements in superalloys*, in *Superalloy 718*1989.

51. Xie, X., *Investigation on High Thermal Stability and Creep Resistant Modified Inco 718 with Conbined Precipitation of γ ″and γ′.* Superalloy 718, 625, 706 and Various Derivatives, 1994. **711**.
52. Chang, S.-H., S.-C. Lee, and K.-T. Huang, *Influences of γ ″and δ Precipitations on the Microstructural Properties of 718 Alloy through HIP, Solid-Solution, and Different Aging Heat Treatments.* Materials transactions, 2010. **51**(9): p. 1683-1688.
53. Hassan, B. and J. Corney, *Grain boundary precipitation in Inconel 718 and ATI 718Plus.* Materials Science and technology, 2017. **33**(16): p. 1879-1889.
54. Byun, T. and K. Farrell, *Tensile properties of Inconel 718 after low temperature neutron irradiation.* Journal of Nuclear Materials, 2003. **318**: p. 292-299.
55. Trosch, T., et al., *Microstructure and mechanical properties of selective laser melted Inconel 718 compared to forging and casting.* Materials letters, 2016. **164**: p. 428-431.
56. Zhao, X., et al., *Study on microstructure and mechanical properties of laser rapid forming Inconel 718.* Materials Science and Engineering: A, 2008. **478**(1-2): p. 119-124.
57. Qi, H., M. Azer, and A. Ritter, *Studies of standard heat treatment effects on microstructure and mechanical properties of laser net shape manufactured Inconel 718.* Metallurgical and Materials Transactions A, 2009. **40**(10): p. 2410-2422.
58. Guimaraes, A.A. and J. Jonas, *Recrystallization and aging effects associated with the high temperature deformation of waspaloy and inconel 718.* Metallurgical transactions A, 1981. **12**(9): p. 1655-1666.
59. Tabernero, I., et al., *Evaluation of the mechanical properties of Inconel 718 components built by laser cladding.* International Journal of Machine Tools and Manufacture, 2011. **51**(6): p. 465-470.
60. Loria, E., *Superalloys 718, 625, 706 and various derivatives.* Pittsburgh, 1994: p. 1994.
61. Dong, J., X. Xie, and R. Thompson, *The influence of sulfur on stress-rupture fracture in inconel 718 superalloys.* Metallurgical and Materials Transactions A, 2000. **31**(9): p. 2135-2144.
62. Liu, Y., et al., *Effects of microporosity and precipitates on the cracking behavior in polycrystalline superalloy Inconel 718.* Materials characterization, 2017. **132**: p. 175-186.
63. Chang, L., et al., *Influences of hot-isostatic-pressing temperature on microstructure, tensile properties and tensile fracture mode of Inconel 718 powder compact.* Materials Science and Engineering: A, 2014. **599**: p. 186-195.
64. Rao, G.A., M. Srinivas, and D. Sarma, *Effect of solution treatment temperature on microstructure and mechanical properties of hot isostatically pressed superalloy Inconel* 718.* Materials Science and technology, 2004. **20**(9): p. 1161-1170.